Research Square

Preprints are preliminary reports that have not undergone peer review.
They should not be considered conclusive, used to inform clinical practice,
or referenced by the media as validated information.

AAV9-Mediated Gene Replacement Therapy for CTNNB1-Related Neurodevelopmental Disorder

Leszek Lisowski

llisowski@cmri.org.au

Children's Medical Research Institute https://orcid.org/0000-0002-4772-8651

Andrea Perez-Iturralde

Children's Medical Research Institute

Dusko Lainscek

National Institute of Chemistry https://orcid.org/0000-0001-9613-5441

Hardik Parate

Children's Medical Research Institute

Charles Morgan

Children's Medical Research Institute

Jingwei Chen

Children's Medical Research Institute

Anna Koudrina

Children's Medical Research Institute

Florencia Haase

Children's Medical Research Institute

Rodney Samaco

Rare Collective Strategies LLC (Rarion) https://orcid.org/0000-0001-5636-5314

José Lanciego

University of Navarra

Estera Zupančič

BIA Separations CRO—Labena d.o.o,

Maddison Knight

Children's Medical Research Institute https://orcid.org/0000-0002-8009-067X

Ana Gonzalez Hernandez

CTNNB1 Foundation

Roman Jerala

National Institute of Chemistry (Slovenia) https://orcid.org/0000-0002-6337-5251

Damjan Osredkar

University Medical Centre Ljubljana

Špela Miroševič

CTNNB1 Foundation

Article

Keywords:

Posted Date: August 27th, 2026

DOI: https://doi.org/10.21203/rs.3.rs-10408032/v1

License: This work is licensed under a Creative Commons Attribution 4.0 International License.
Read Full License

Additional Declarations: Yes there is potential Competing Interest. The CTNNB1 Foundation holds an exclusive global license to the international patent application WO2025/094056 (“Gene Therapy for CTNNB1 Syndrome”), filed by Children’s Medical Research Institute. ŠM is the founding president of the CTNNB1 Foundation and LL, API, CM and JC are listed as inventors on the patent application. The other authors declare no competing interests.

AAV9-Mediated Gene Replacement Therapy for *CTNNB1*-Related Neurodevelopmental Disorder

Perez-Iturralde, A.[1,†], Lainšček, D. [2,3,4,5,†], Parate, H.[1], Morgan, C.W.[1], Chen, J.[1], Koudrina, A.[1], Haase, F.D.[1], Samaco, R.C.[6], Lanciego, J.L.[7], Zupančič, E.M.[8], Knight, M.[1], Gonzalez Hernandez, A.[9,10], Jerala, R.[2,3], Osredkar, D.[11,12], Miroševič, S.[5, 10, 13,‡*], Lisowski, L.[1,5,14,15,‡,*].

† Authors contributed equally to this work and share the first authorship.

‡ Authors contributed equally to this work and share the senior authorship.

[1]Translational Vectorology Research Unit, Children's Medical Research Institute, Faculty of Medicine and Health, The University of Sydney, Westmead, NSW 2145, Australia.

[2]Department of Synthetic Biology and Immunology, National Institute of Chemistry, Ljubljana, 1000, Slovenia.

[3]Centre for Technologies of Gene and Cell Therapy, National Institute of Chemistry, Ljubljana, 1000, Slovenia.

[4]Veterinary Faculty, University of Ljubljana, Ljubljana, 1000, Slovenia

[5]Gene2Cure Foundation, Foster City, 94404, California, United States

[6]Rare Collective Strategies LLC (Rarion), Chicago, Illinois, United States

[7] CNS Gene Therapy Program, Center for Applied Medical Research (CIMA), University of Navarra, Pamplona, Spain

[8]Molecular Biology Laboratory, BIA Separations CRO—Labena d.o.o, Ljubljana, 1000, Slovenia

[9]Asociación CTNNB1 España, Basauri, 48970, Spain.

[10]CTNNB1 Foundation, The Gene Therapy Research Institute, Ljubljana, 1000, Slovenia.

[11]Department of Pediatric Neurology, University Children's Hospital, University Medical Centre Ljubljana, 1000 Ljubljana, Slovenia.

[12]Department of Pediatrics, Faculty of Medicine, University of Ljubljana, Ljubljana, 1000, Slovenia.

[13]Department of Family Medicine, Faculty of Medicine, University of Ljubljana, Ljubljana, 1000, Slovenia.

[14]Australian Genome Therapeutics Centre, Children's Medical Research Institute and Sydney Children's Hospitals Network, Westmead, NSW 2145, Australia.

[15]Laboratory of Molecular Oncology and Innovative Therapies, Military Institute of Medicine - National Research Institute, Warszawa, Poland.

*Corresponding authors:

Leszek Lisowski, Children's Medical Research Institute, Westmead NSW 2145, Australia. (+61) 4 2833 8594, llisowski@cmri.org.au

Špela Miroševič, Dalmatinova ulica 5, 1000 Ljubljana, Slovenia. (+386) 31 731 269, spela@ctnnb1-foundation.org

Abstract

CTNNB1 Syndrome is a severe neurodevelopmental disorder caused by haploinsufficiency of the *CTNNB1* gene, which encodes β-catenin, a central regulatory protein of the canonical Wnt signaling and nervous systems development. Today affected patients experience global developmental delays (GDD), intellectual disability, and progressive motor impairments, with no disease-modifying treatment available. We developed and evaluated the first gene therapy targeting CTNNB1 Syndrome based on recombinant adeno-associated virus (rAAV). Six therapeutic cassettes were engineered and screened in patient-derived cortical brain organoids, identifying the lead candidate that restores β-catenin function with downstream pathway normalization. The selected vector was evaluated in a mouse model recapitulating motor and behavioral symptoms of the CTNNB1 Syndrome patients. To do so, juvenile CTNNB1 Syndrome mice received escalating unilateral intracerebroventricular doses of the vector. Mice treated with the highest dose showed improved locomotor and anxiety-related behaviors, with no adverse effects over eight months. Drug material for toxicology and biodistribution studies was manufactured under current Good Manufacturing Practice (cGMP) conditions. Safety, biodistribution and tolerability were further assessed in wild-type mice and non-human primates (NHPs), of which some mice toxicology and biodistribution analyses were conducted under Good Laboratory Practice (GLP) and in compliance with the European Medicines Agency (EMA) regulatory requirements. Following infusion of animals with the drug candidate, no treatment-related clinical, biochemical or histopathological adverse findings were observed and the No Observed Adverse Effect Level (NOAEL) was established at the highest vector dose. These findings support the preclinical safety and therapeutic efficacy in AAV9-mediated β-catenin gene augmentation therapy, paving the way for a clinical trial in Europe, already initiated in December 2025.

Introduction

CTNNB1 Syndrome is a severe neurodevelopmental disorder with an estimated incidence of 2.6-3.2 per 100,000 live births (1). It is characterized by intellectual disability, global developmental delay (GDD), autistic features, learning difficulties, progressive spasticity and motor disabilities (2,3). While clinical manifestation differs between subjects, several patients exhibit microcephaly, retinal (4) and cardiac abnormalities (5). The rarity of CTNNB1 Syndrome, combined with phenotypic overlap with conditions such as cerebral palsy (CP) (6), led to widespread misdiagnosis and delayed its recognition as a distinct condition. Recently, exome sequencing based meta-analysis confirmed *CTNNB1* mutations as one of the leading genetic etiologies for cerebral palsy (7), indicating a higher than previously assumed incidence of the disease.

CTNNB1 Syndrome was first described in 2012 (8) as an autosomal dominant monogenic haploinsufficiency condition typically caused by single allele *de novo* loss-of-function mutations in the *CTNNB1* gene, which encodes for the β-catenin protein.

Beta-catenin is essential for embryonic development, maturation of the central and peripheral nervous systems (CNS and PNS), and normal functioning of the brain in adulthood (9–12). Additionally, β-catenin is a central effector protein in canonical Wnt signaling pathway. Beta-catenin acts at multiple sites in the nervous system. In the plasma membrane, β-catenin links pre- and post-synaptic neurons through its interaction with N-cadherins, playing a role in synaptic vesicle formation, plasticity, learning, and memory consolidation (13–16). In the nucleus, β-catenin recruits chromatin-remodeling proteins and interacts with transcription factors TCF/LEF, promoting transcription of *Wnt*-regulated genes such as *MYC*, *CCDN1*, or *AXIN2* (17), with roles in cell proliferation, cell adhesion via cadherin-to-cadherin interactions, cell determination (9,10), astrocyte differentiation, glial activation (18), axon guidance and formation of the synapses between motor neurons and muscle cells (neuro-muscular junctions) (19,20). In addition, β-catenin protein plays an important role in formation of the blood-brain barrier (BBB) (21).

Importantly, *CTNNB1* has emerged as a high-confidence risk gene for autism spectrum disorder (ASD) (22–24). Dysregulation of Wnt/β-catenin signaling during neurodevelopment disrupts cortical patterning, neuronal proliferation, and synaptic function-processes strongly implicated in ASD pathogenesis (24). Accordingly, ASD features are highly prevalent among individuals

with CTNNB1 Syndrome, making it a compelling monogenic model for investigating the molecular mechanisms of autism.

With no current treatments available and the limited interest from the pharmaceutical industry in developing therapies for rare genetic conditions, the quality of life of individuals with CTNNB1 Syndrome progressively deteriorates, highlighting a high unmet medical need. Current research has been focused on the use of small molecules that target and inhibit the degradation complex responsible for the downregulation of β-catenin protein (25). Additionally, mutation-independent correction of *CTNNB1* mRNA levels has been achieved through spliceosome-mediated RNA *trans*-splicing (26), highlighting a promising therapeutic strategy.

Since all features of CTNNB1 Syndrome are driven by a reduced production of functional β-catenin protein, we hypothesized that a gene augmentation therapy, aiming to deliver a functional copy of the gene to complement the sub-physiological levels of the functional protein, could offer the first disease-modifying therapeutic strategy for CTNNB1 Syndrome.

Recombinant adeno-associated viruses (rAAVs) are emerging as highly promising vectors in the field of gene therapy, as they are able to confer long-term episomal expression in non-dividing cells, such as neurons (27), with a minimal risk of insertional mutagenesis (28,29). These vectors are derived from non-pathogenic parvoviruses with a single-stranded DNA genome of approximately 4.7 kilobases (kb), flanked by palindromic ~145 nt Inverted Terminal Repeats (ITRs) that serve as origin of replication and are required for vector packaging (28). Given that ITRs are the only elements required *in cis* for genome packaging (30), the remaining elements of the AAV genome can be removed, thereby maximizing space (~4.4 kb) for the therapeutic cassette. This design ensures that rAAVs lack all the elements required for viral replication, thus enhancing safety profile of AAV-based therapies. AAV vectors have already demonstrated high efficacy and safety for the treatment of several conditions, including spinal muscular atrophy (SMA) (Zolgensma®), for which high efficiency and safety was shown (31).

In this study, initiated by the CTNNB1 Foundation, a patient-leading non-for-profit organization, a set of six AAV-CTNNB1 constructs containing different combinations of regulatory elements were engineered and developed for the selection of the most promising therapeutic candidate. Restoration of β-catenin function was firstly confirmed in patient-derived cortical brain organoids. The therapeutic efficacy of the selected AAV-CTNNB1

construct was further evaluated in a project generated *Ctnnb1*$^{+/-}$ murine model, where recovery in locomotor function and anxiety-like behavior, two key phenotype features frequently manifested by CTNNB1 Syndrome patients, was observed. To study the safety profile of the therapeutic vector, an 8-month non-good laboratory practice (non-GLP) toxicology study was conducted in naive C57BL/6J mice, followed by comprehensive histopathological evaluation. Subsequent safety and biodistribution assessment were performed following EMA guidelines for new drug development. To do so, an AAV-CTNNB1 vector batch was produced under current Good Manufacturing Practice (cGMP) conditions. Toxicology and biodistribution analyses were performed in mice (3-month GLP study) and non-human primates (NHPs) (3-month non-GLP study). A comprehensive study confirmed absence of treatment-related pathological changes, as determined by clinical observations, clinical chemistry parameters and final histopathology assessment.

Together, these studies demonstrate the potential therapeutic effects of the AAV9-CTNNB1 vector with no evidence of treatment-related toxicity. These studies supported the Phase I/II investigational gene therapy clinical trial for CTNNB1 Syndrome (EUCT number: 2025-522719-40-00), which was initiated in Slovenia in December 2025.

Results

Design and validation of AAV-CTNNB1 expression cassettes

CTNNB1 Syndrome is predominantly caused by haploinsufficiency of β-catenin; therefore, restoring physiological protein levels through AAV-mediated gene delivery of a functional copy of the gene represents a rational therapeutic strategy. To identify the most effective configuration of the *CTNNB1* coding region and regulatory elements, six therapeutic cassette candidates encoding the *CTNNB1* gene under the control of the cytomegalovirus enhancer/chicken β-actin hybrid (CBh) promoter were engineered (Fig. 1a). Since AAV vectors can accommodate genome sizes of up to 4.4 kb (28) and the length of *CTNNB1* coding region is 2,343 nt (β-catenin is 781aa), additional regulatory sequences were incorporated to optimize transgene expression. These included 5' and 3' untranslated regions (UTR) and intronic fragments derived from the endogenous *CTNNB1* gene. Different variants of *CTNNB1* coding DNA sequences (CDS) were also investigated, including a codon optimized (COP) version and a truncated version lacking the last 108 amino acid residues of β-catenin carboxy-

terminal domain (ΔCTD), containing the transactivation domain required for β-catenin's nuclear activity (32).

AAV vectors have been linked to toxicity in the liver and dorsal root ganglia (DRG) of large animal models, such as piglets and NHPs (33). As this effect has been largely attributed to off-target transgene overexpression, the post-transcriptional silencing of the vector transcripts in these tissues was evaluated by incorporating microRNA Targeting Sequences (miRTS) (34) into the AAV cassette. To do so, a mix of miRTS was designed containing binding sites for miR122a-5p and miR199a-5p, to induce posttranscriptional silencing in the liver, and miR183-5p, to lead to transgene silencing in the DRG. Each miRTS was incorporated in triplicate. Based on *in vivo* optimization studies (data not shown), the selected configuration consisted of nine tandem repeats arranged in "A-B-C-A-B-C-A-B-C" pattern, without linker sequences between sites. In this design, "A" corresponds to miR122a-5p, "B" to miR183-5p, and "C" to miR199a-5p. For functional validation, this miRTS detargeting element was inserted into a control AAV cassette between the enhanced Green Fluorescent Protein (eGFP) reporter gene and the bovine growth hormone polyadenylation signal (pA) (Supplementary Fig. 1a). The cassette was packaged into an AAV9 vector and intravenously inoculated into *Fah*$^{-/-}$/*Rag2*$^{-/-}$/*Il2rg*$^{-/-}$ (FRG) (35) chimeric mice repopulated with primary human hepatocytes. An AAV9-eGFP vector lacking miRTS was used as control. As shown in Supplementary Fig. 1a, a dramatic reduction in the expression of the eGFP reporter was observed in liver and dorsal root ganglia when the miRTS detargeting elements was included, while no impact on eGFP expression was observed in the control group four weeks post-inoculation. Therefore, this set of miRTS was added to all the AAV-CTNNB1 constructs to limit off-target activity and increase the safety profile of the resulting vectors.

For initial functional validation, each AAV-CTNNB1 construct was packaged into the AAV2.7m8 capsid (36) and evaluated in *CTNNB1*-knockout (KO) HEK-293T cells generated in-house (Supplementary Fig. 1b). To do so, cells were transduced with 2.00×10^6 vector genomes (vg)/cell and harvested 96 hours post-transduction. Quantitative gene expression analysis demonstrated that constructs C1, C2, and C3 restored *CTNNB1* mRNA to levels comparable to the wild-type control, whereas construct C4 induced supraphysiological expression. In contrast, constructs C5 failed to rescue *CTNNB1* transcript levels (Supplementary Fig. 1c). At the protein level, western blot analysis revealed that even though protein expression levels were increased after AAV2.7m8-CTNNB1 transduction, at the vector

dose used, none of the constructs was able to restore physiological levels of β-catenin protein (Supplementary Fig. 1d-e). Consistent with the deletion of the carboxy-terminal end present in C3's CDS (Fig. 1a), construct C3 expressed a shorter form of β-catenin (Supplementary Fig. 1d).

AAV2.7m8-CTNNB1(C4) corrects phenotypes in patient-derived cortical brain organoids

Following this initial validation, we next sought to identify the optimal AAV-CTNNB1 cassette configuration in cortical brain organoids derived from a patient with CTNNB1 Syndrome (*CTNNB1^mut^*). RT-qPCR analysis confirmed that CTNNB1 mRNA levels were markedly reduced in *CTNNB1^mut^* relative to healthy control (HC)-derived organoids (Supplementary Fig. 1f), and with concomitant reduction in β-catenin protein expression confirmed with immunostaining (Supplementary Fig. 1g, h). Given the central role of β-catenin in synaptic and astrocytic biology (13,18,34), synaptophysin and glial fibrillary acidic protein (GFAP) were also evaluated and were both reduced in *CTNNB1^mut^* organoids, although the limited sample size precluded statistical analysis. Together, these findings indicate that *CTNNB1^mut^* organoids recapitulate key molecular features of CTNNB1 Syndrome.

To compare the different AAV-CTNNB1 cassettes in this preclinical model, the AAV2.7m8 capsid was used as a surrogate AAV variant, as it has previously been shown to outperform wild-type AAV serotypes 1-12 and other bioengineered capsids at transduction of cortical brain organoids (27). Organoids were transduced at a multiplicity of transduction (MOT) of 1×10^{10} vg per organoid and harvested two weeks later for downstream analysis (Fig. 1b). RT–qPCR and immunostaining analyses identified C4 as the lead construct, as it was the only cassette that increased *CTNNB1* mRNA expression to levels comparable to those observed in HC organoids (Fig. 1c).

RNA-seq (Supplementary Fig. 2) was performed on organoids following treatment with AAV2.7m8-CTNNB1(C4) to fully determine the pathway activation upon β-catenin protein restoration. Within this framework, AAV2.7m8-CTNNB1(C4) treatment was associated with increased *CTNNB1* expression across organoids (Supplementary Fig. 3a), together with directional changes in expression of Wnt/β-catenin-related genes (Supplementary Fig. 3b) and cell adhesion-associated genes (Supplementary Fig. 3c), consistent with partial restoration of

β-catenin-dependent transcriptional pathways. Examination of expression of selected β-catenin pathway genes, including *CTNNB1*, *AXIN2*, *LEF1*, *TCF7*, *GSK3B* and *CDH2*, further supported a treatment-associated shift in pathway-relevant gene expression, although the magnitude and direction of change varied across genes and lines (Supplementary Fig. 3d).

Given the established association between β-catenin and tumorigenesis (37), the same transcriptomic dataset was used to assess whether treatment-induced gene expression changes were associated with oncogenic risk. Gene set variation analysis indicated that AAV2.7m8-CTNNB1(C4) did not trigger aberrant activation of safety-relevant proliferation or stress-associated pathways (Supplementary Fig. 4a). Across cell cycle-linked signatures, including E2F targets, G2M checkpoint and MYC targets (38), pathway scores in treated organoids remained comparable to, or lower than, those observed in untreated controls. Similarly, PI3K/AKT/mTOR, apoptosis and p53 pathway signatures showed no evidence of marked induction beyond the range observed across control organoids. Together, these data provide no transcriptomic evidence of broad oncogenic activation or unintended stimulation of proliferation-associated pathways, supporting a favorable molecular safety profile for this AAV-mediated gene therapy.

Pathway-level analyses further supported partial correction of β-catenin-dependent neurodevelopmental processes. Treatment was associated with directional changes in expression of genes involved in neuronal maturation (Supplementary Fig. 4b) and genes associated with glutamatergic synapse (Supplementary Fig. 4c), consistent with partial restoration of transcriptional pathways linked to neuronal differentiation, connectivity and synaptic function. These findings are in agreement with the established role of β-catenin in neuronal maturation, cell adhesion and synapse organization (13,37), and support the interpretation that AAV2.7m8-CTNNB1(C4) promotes molecular recovery without broader pathway disruption.

Consistent with these transcriptomic findings, AAV2.7m8-CTNNB1(C4) also restored β-catenin, synaptophysin and GFAP protein expression in *CTNNB1* ^{mut} organoids (Fig. 1d and Supplementary Fig. 5, Supplementary Fig. 6), further supporting the therapeutic potential of the selected AAV-CTNNB1 candidate for the treatment of CTNNB1 Syndrome.

CTNNB1 Syndrome disease mouse model generation

To evaluate the therapeutic effect of AAV9-CTNNB1(C4) gene replacement therapy *in vivo,* an efficacy study was performed in a mouse model of CTNNB1 Syndrome. As the majority of CTNNB1 Syndrome patients are heterozygotes for loss-of-function variants (3,37), a whole-body loss of β-catenin function mouse was generated (Supplementary Fig. 7a), as homozygous whole-body *Ctnnb1* KO mice are not viable (39,40).

Comprehensive characterization studies of this new murine model showed reduced β-catenin protein levels in both the central nervous system (CNS) and peripheral tissues (Supplementary Fig. 7b), together with reduced growth relative to wild-type littermates (Supplementary Fig. 7c). Contextual fear conditioning (CFC), an assay used to assess associative learning and memory (41) showed that mutant mice exhibited increased freezing behavior compared to controls, with a more pronounced effect in males (Supplementary Fig. 7d-e). An additional phenotype in male mice was identified using the Rotarod Test, which assesses motor coordination, balance and endurance (42). This analysis showed that male mice displayed reduced motor performance at younger ages, followed by recovery over time (Supplementary Fig. 7d-e).

AAV9-CTNNB1(C4) *in vivo* efficacy study

Beta-catenin$^{+/-}$ mice and their wild-type littermates were subsequently used in an efficacy study, a key step in preclinical drug development (43). Considering the fact that CTNNB1 Syndrome is a neurodevelopmental condition (2), intracerebroventricular (ICV) route of administration was selected for vector delivery, as based on published data and discussion with key opinion leaders (KOL) (data not shown), ICV administration can achieve broader and more extensive brain transduction compared to other delivery routes (44–46).

Juvenile *Ctnnb1*$^{+/-}$ mice were infused ICV with low (4.24×10^9 vg/mouse), mid (2.12×10^{10} vg/mouse) or high doses (1.06×10^{11} vg/mouse) of the AAV9-CTNNB1(C4) vector. To control for potential effects of vector delivery alone, AAV9-eGFP vector (2.13×10^{10} vg/mouse) was administered ICV to heterozygous mutant and wild-type animals. Therapeutic efficacy was assessed using a broad battery of behavioral assays through 23 weeks of age (Fig. 2a), at which point the study was terminated and tissues were collected for molecular analyses.

The treatment with experimental gene therapy had no adverse effects on general development, as the body weight in both male and female mice increased throughout the study (Supplementary Fig. 8a). In the Marble Burying Test, which assesses anxiety-like and compulsive-like behavior, both males and females showed a transient behavioral improvement after AAV9-CTNNB1(C4) treatment at 12 weeks of age, although this difference was not maintained at later timepoints (Supplementary Fig. 8b).

The clearest rescue of the disease phenotype was observed in the Open Field Test and in kinematic gait analysis. The overall spontaneous locomotor activity of the *Ctnnb1*$^{+/-}$ mice was reduced, with a more pronounced effect in males than in females, as indicated by decreased horizontal activity starting at 4 weeks and reduced vertical activity from 12 weeks onward. Treatment with the high dose of AAV9-CTNNB1(C4) significantly increased rearing activity in the Open Field Test compared with AAV9-eGFP-treated mutant mice (Fig. 2b, Supplementary Fig. 8c).

Kinematic Gait Analysis enabled detailed assessment of gait pattern, posture, balance and fine motor control, features that are also affected in individuals with CTNNB1 Syndrome (3,47). *Ctnnb1*$^{+/-}$ mice exhibited notable motor deficits and alterations, including a lowered back posture evidenced by reduced tail base, iliac crest, and hip height positions, as well as changes in joint angles and the movement trajectories of the hind and fore paws during the swing phase, compared to wild-type mice (Supplementary Fig. 9a). Treated mice demonstrated improvements in several fine motor parameters, such as paw trajectory, fine tail positioning etc. Administration of mid and high doses of AAV9-CTNNB1(C4) significantly improved the overall gait score at 12 weeks of age in females and at 20 weeks of age in males. Additionally, certain gait features (such as hip angle, stride time, or protraction of hind limb) also showed improvement at 20 weeks in the both sexes group of sexes after the treatment (Fig. 2c, Supplementary Fig. 9b-f).

Contextual Fear Conditioning also showed a moderate treatment-associated improvement (Fig. 2d), whereas all other behavioral assays, including Clasping and Radial Arm Water Maze Testing, did not reveal significant treatment-related differences.

At 23 weeks of age, 19 weeks after the treatment, animals were sacrificed and various tissues were collected for analysis. Functional transduction of the brain was assessed by measuring *hCTNNB1* transgene expression and subsequent increase in β-catenin protein. RT-qPCR

analysis showed a dose-dependent increase of *hCTNNB1* mRNA across multiple brain regions (Fig. 2e-f, Supplementary Fig. 10a). A significant increase of the β-catenin protein was observed in AAV9-CTNNB1(C4)-treated animals in various brain regions (Fig. 2g-h, Supplementary Fig. 10b), whereas peripheral increase of the protein in off-target tissue (liver, muscles) was not observed (Supplementary Fig. 10c). Biochemical profiling, performed to assess the effects of treatment on systemic homeostasis and liver and kidney function, showed no evidence of toxicity, as all measured parameters remained unchanged in treated animals comparing to controls (Fig. 2i-k, Supplementary Fig. 10d-f).

AAV9-CTNNB1(C4) gene therapy does not lead to long-term toxicity in mice

To assess the long-term safety and the potential impact of β-catenin overexpression following AAV9-CTNNB1(C4) treatment, 28±3-day-old wild-type C57BL/6J mice were ICV inoculated with 1.06×10^{11} or 2.25×10^{11} vg/mouse of the drug candidate or the control (AAV9-eGFP) vector and monitored for eight months (Fig. 3a). Age and sex matched untreated wild-type mice served as controls.

Animals were evaluated weekly for behavior, physical appearance, and body weight to identify any potential adverse effects. Growth trajectories were unaffected by the inoculation with either AAV9-CTNNB1(C4) or AAV9-eGFP vectors (Fig. 3b), and body weight changes were similar between groups (Fig. 3c). Moreover, no behavioral alterations were observed throughout the study.

Blood samples were collected one week and three months post-injection as well as at the time of sacrifice to assess biochemical markers indicative of liver, kidney, and bile duct function. Analysis showed (Supplementary Fig. 11a-c) that no statistically significant differences were detected in albumin, alanine aminotransferase (ALT), alkaline phosphatase (ALP), total protein, total bilirubin, or creatinine among the untreated, AAV9-eGFP control, and AAV9-CTNNB1(C4)-treated groups, confirming a lack of treatment-related toxicity.

Upon sacrifice, no macroscopic anomalies were observed in any animals. Histopathological examination of brain and peripheral tissues revealed no treatment-related alterations. In the liver, microvesicular steatosis and extramedullary hematopoiesis were present across all groups, including untreated animals, suggesting these findings were age-related and unrelated

to treatment. In the brain and cerebellum, sporadic observations such as neuronal degeneration, vacuolation, and intramyelinic edema were noted but were attributed to tissue-processing artifacts rather than treatment-induced toxicity. Cortical thickness (Fig. 3d) was generally comparable between treated and control animals; however, a modest yet not statistically significant increase was detected in female mice administered 2.25×10^{11} vg of control AAV9-eGFP vector and not within group treated with therapeutic candidate vector. Collectively, these findings demonstrate that administration of up to 2.25×10^{11} vg of AAV9-CTNNB1(C4) does not induce any adverse behavioral, biochemical, or histopathological effects in wild-type mice.

Production of cGMP-like grade AAV9-CTNNB1(C4) viral vector

For the safety and biodistribution assessment of the AAV9-CTNNB1(C4) vector in rodent and non-rodent animal models, a non-clinical batch of the vector was produced. This non-clinical 50 L batch, referred to as Urbagen Lot T-CRUX-110, was manufactured in a cGMP-certified facility following current European Pharmacopeia and EMA guidelines (48–52).

Before initiating animal studies additional confirmation of Urbagen identity was performed. Specifically, identity of AAV9 capsid proteins (VP1, VP2 and VP3) was determined via western blot and specific immunodetection (Supplementary Fig12a). Additionally, comparability study between research grade AAV9-CTNNB1(C4) and cGMP-like grade Urbagen was conducted, revealing no significant differences at the vector DNA and vector-derived mRNA expression levels (Supplementary Fig. 12b). Additionally, a potency assay using *CTNNB1* KO cells confirmed that the batches were comparable in efficacy (Supplementary Fig. 12c-d).

GLP compliant safety study in mice

To evaluate the safety of the Urbagen, a 90-day GLP regulatory enabling toxicology study was performed (n=10 animals per sex; 4 groups, total of 80 animals). In this study, 28 days old male and female wild-type mice received ICV infusion of Urbagen at three different doses: 5.00×10^{10} vg/mouse (the low dose), 1.00×10^{11} vg/mouse (the medium dose), and 3.35×10^{11} vg/mouse (the high dose). All vector doses were adjusted to ensure equal vector volumes in all

three groups. The high dose represented also the Maximum Feasible Dose (MFD) based on the vector titer and injection volume limitations. Control group animals received the same volume of vehicle (cGMP-like PBS solution, containing Poloxamer 188) only. During the toxicology study, animals were monitored twice a day for potential mortality, gross clinical observation (Supplementary Table 1) focusing on animal activity and movement, body posture, coat and body condition, vocalization of the animals, respiration, body weight (measured weekly), hydration status, secretion observation. In addition, visible mucosae surveillance was carried out daily, whereas detailed clinical observation scoring of each animal was conducted once per week. Feed and water consumption were monitored. As several CTNNB1 Syndrome patients can develop eye pathologies or even Familial Exudative Vitreoretinopathy (FEVR) that can result in blindness (4), ophthalmological examinations (Supplementary Table 2) were conducted in order to assess the potential toxicity of Urbagen in the eye. The eye exam was performed before the ICV administration of the drug candidate and before the necropsy of the animals. Finally, at study termination, major organs, including brain, liver, spleen, pancreas, gonads etc. were harvested for a scoring-based (Supplementary Table 5) histopathology analysis. (Fig. 4a).

During the 90-day toxicology study, no significant changes in body weight were observed, neither in male nor female animals, after ICV AAV-CTNNB1(4) inoculation. In fact, all animals gained weight at a similar rate to control animals and as expected based on their normal age-related growth and development (Fig. 4b, Supplementary Fig. 13a). During the study period, most animals across all groups exhibited a normal clinical condition (score 0). The most commonly observed clinical signs (Supplementary Table 6) included mild, localized coat alterations such as barbering, alopecia, minor scabs, or wounds from fighting (especially among co-housed males due to frequently reported in mice inter-male aggression). Mild ocular changes, mainly corneal opacity, were observed across all groups, including controls. Occasionally and transiently, animals displayed signs such as increased respiratory rate, hypoactivity, or stress-related behaviors, but these were limited to isolated cases. Female survival rate in the 90-day toxicity study was 100% for all test groups. In contrast, two male animals in the medium dose group (1.00×10^{11} vg/mouse) met humane endpoint criteria (total clinical score >5) and were euthanized prior to scheduled necropsy (on days 26 and 57 of the study) due to progressive deterioration, leading to overall 80% survival rate in the male medium dose group and 100% survival for all other male dose groups (Fig. 4c).

One animal showed head swelling. Necropsy analysis of this animal revealed multiple multisystem abnormalities, including pronounced hydrocephalus with asymmetric brain shape and enlarged skull, subdural hemorrhage, and red exudate likely from intracranial hypertension. Additional findings included intestinal pathology, enlarged lymph nodes indicating immune activation, absence of internal fat, a reduced thymus, and underdeveloped seminal vesicles, reflecting poor overall health.

All surviving animals (n=78) were subjected to terminal necropsy procedures on day 90 and underwent a complete post-mortem examination. Gross examination revealed various macroscopic findings in both control and treated groups. These included a speckled liver texture observed across all groups, pale livers in some low and medium dose group animals, and dark spots present on certain livers. Spleen melanosis was seen in multiple animals, while some animals exhibited reduced spleen size. Heart enlargement was noted in a few animals, along with hyperemia in isolated cases. Slight kidney enlargement, alopecia, barbering affecting the skin and hair, and isolated instances of megacolon and cataracts were also recorded (Supplementary Table 7).

Hematological analysis was performed on all surviving animals. A complete blood count (CBC) with differential was conducted to assess their hematological status. Blood analysis revealed no signs of inflammation or erythropoiesis malfunction in treated animals, as all blood cell counts and blood panel values were within normal ranges (Fig. 4d-e, Supplementary Fig. 13b). Coagulation assays, measuring prothrombin time and activated partial thromboplastin time (APTT), additionally confirmed that administration of AAV9-based Urbagen did not cause any coagulopathies as all measured values were similar throughout all treatment groups (Fig. 4f). As liver toxicity is one of the most common side effects of AAV9-based therapies (53) a clinical blood chemistry was performed, where several factors suggested normal homeostasis liver and kidney functions. Additionally, the absence of liver toxicity was further confirmed by unchanged albumin, total protein, ALT, aspartate aminotransferase (AST) and ALP values, whereas creatinine kinase, urea and ions unaltered levels confirmed lack of kidney malfunctions (Fig. 4g, Supplementary Fig.14). In blood measurements across all groups, physiological variability was observed with no consistent dose-dependent alterations attributable to the tested item. Additionally, urinalysis (pH, presence of bacteria, blood, ketone bodies, glucose) showed no treatment-related abnormalities, further confirming the absence of Urbagen-induced systemic toxicity (data not shown).

As mentioned above, ophthalmological exam was also carried out on all animals. Although some changes in specific ophthalmological parameters were observed, these findings appeared sporadically across all groups, including the controls, and were deemed incidental. The most significant variation was seen in corneal cloudiness, especially in terms of severity score and the affected area (Supplementary Fig. 15).

A systematic histopathological analysis of H&E-stained tissue sections was performed. In the examined organs, no consistent dose-dependent trends or pathological patterns were observed that would indicate systemic toxic effects of Urbagen. Particular emphasis was placed on the histopathological assessment of the brain. Analysis of brain tissues across all groups after ICV administration of Urbagen showed mostly minimal to moderate (Grade 0–2) focal changes. The most common lesions: periventricular inflammation, perivascular edema, and occasional focal necrosis and hemorrhages, were primarily near the injection site, indicating these were mainly due to mechanical trauma and localized immune responses rather than direct neurotoxicity of the test item (Fig. 4h).

The majority of the findings were of minimal to mild severity (Grades 1–2) and appeared with similar frequencies in both treated and control animals. Retinal dysplasia and pituitary cysts occurred sporadically in both groups without dose-related trends. Minor villous degeneration in the small intestine segments was also observed in both high dose and control animals, with no link to the test item. Mild inflammatory infiltrates or acinar degeneration in the liver, pancreas, and lymph nodes were incidental, showing no tissue damage or impairment. Age-related adrenal hyperplasia and spleen extramedullary hematopoiesis were present in both groups. Testicular germ cell changes were minimal and seen in both high dose and control groups, with no spermatogenic arrest. Spinal cord findings, including demyelination and edema, were sporadic and also occurred in controls, indicating no test item association. Importantly, no histopathological evidence of systemic inflammation, necrosis, hemorrhage, or degenerative changes attributable to the test item was observed in any non-neural tissue (Fig. 4i, Supplementary Table 8, Supplementary Fig. 16).

As previously noted, two male mice in the medium dose group were humanely euthanized on days 26 and 57 of the study, as they exhibited significant body weight loss, labored irregular breathing, apathy, tremors, and incoordination. Histopathological review of tissue samples of the these two mice revealed severe hydrocephalus, edema, hemorrhage, neuronal degeneration, and spinal demyelination. The gastrointestinal tract had widespread epithelial hyperplasia,

villous atrophy, ulceration, and inflammation. The liver was atrophic, and the pancreas exhibited acinar necrosis. Lymphoid organs showed atrophy and immune suppression, including thymic necrosis and bone marrow hypocellularity. The cardiovascular system had cardiomyocyte vacuolation and myocardial necrosis. Kidneys and testes showed tubular degeneration and germ cell loss (Supplementary Table 9).

GLP and GLP-like biodistribution studies in mice

In addition to the safety aspect of Urbagen, the pharmacodynamics and pharmacokinetics of the tested item was determined. Several *in vivo* mouse studies were performed using the cGMP-like preparation of the drug candidate. These studies included a 28-day non-GLP biodistribution study, a 90-day and a 180-days GLP biodistribution study (Fig. 4a). Again, 28 days old male and female wild-type mice received ICV infusion of the same doses of Urbagen, similar as in the toxicology study.

To determine the biodistribution profile of Urbagen, a 90- / 180-day biodistribution study (n=6 animals per sex, with 24 animals in the 90-day study and 24 animals in the 180-day study), and a 28-day GLP-like biodistribution study (n=6 animals per sex; total of 24 animals), were performed. During the study, animals were monitored, examined and scored by the same protocol as in the toxicology study. At the end of each study, which corresponded to 28-, 90- and 180-days post AAV-CTNNB1(C4) administration depending on the study, body fluids, feces and tissue were collected for thorough hematology, biochemical blood analysis, urinalysis and droplet digital PCR (ddPCR)-based determination of vector and *CTNNB1* transgene organism biodistribution.

Daily clinical monitoring of animals after Urbagen administration was performed to assess general clinical signs, morbidity, and mortality with particular attention to tremors, convulsions, salivation, diarrhea, lethargy, sleep, and coma. No adverse clinical signs were observed in all treatment groups, and all animals survived until the scheduled termination (Supplementary Fig.17a). Body weight of the treated animals was not affected and naturally increased slightly during the 28-day observation period, similar to the control group (Supplementary Fig. 17b-d). No pathological findings were detected during external and macroscopic examination at necropsy.

At termination, samples were collected and used for non-GLP biodistribution analysis as approved in ICH guidelines (51). Vector DNA was detected in all organs/tissues tested, with strong positive correlation observed between provector level and vector dose (Fig. 5a). In the CNS, the highest vector DNA concentration was detected in hippocampus and at the injection site, although values in other parts of the brain (brainstem, cerebellum, cortex, thalamus) and in all dorsal root ganglia (DRG) and spinal cord regions were similar. In peripheral tissues, the liver and spleen contained the highest vector DNA levels, followed by the adrenal glands. Vector DNA levels in gonads were almost in all cases below the level of detection (LOD).

The same pattern of biodistribution was determined for human *CTNNB1* mRNA, where again the highest values were detected in hippocampus and liver (Fig. 5b). Transgene expression was detected throughout all CNS regions, while in peripheral tissues, detectable expression was limited primarily to the liver and, to a minor extent, the gonads.

In the 90- and 180-day biodistribution studies, no animals showed morbidity, signs of pain or significant distress during the study, and all animals survived until the scheduled necropsy. Minor findings were observed, including localized coat changes such as alopecia, barbering as well as mild ocular changes (Supplementary Table 10). Body weight of the treated animals was not affected and increased across all animal groups as expected based on the age of the animals (Supplementary Fig. 18). No specific pathological findings were detected during macroscopic examination at necropsy. The most frequently observed findings included spleen enlargement and melanosis, occasional ocular opacities (cataracts), and sporadic increases in visceral fat. Other isolated observations comprised small skin lesions (such as barbering or alopecia), single cases of lymph node enlargement, as well as enlargement of the heart, seminal vesicles, and uterus (Supplementary Tables 11 and 12).

Vector genome analysis by ddPCR confirmed that the 3- and 6-months biodistribution patterns closely resembled the 1-month observations, but with overall lower vector DNA levels. Consistent with the 1-month study, at 3 and 6 months the highest vector DNA levels were again seen in hippocampus and at the injection site. High levels were also confirmed in liver, but at these later time points no vector DNA was detected in gonads, blood and feces. Similarly, vector DNA levels in kidney, spleen and adrenal glands decreased substantially (Fig. 5a). Analysis of *hCTNNB1* mRNA at 3 and 6 months, showed continued expression in cortex, heart and liver (Fig. 5b).

529

530 **Urbagen pharmacokinetics in non-human primates**

531 Finally, the safety and biodistribution of Urbagen was evaluated *in vivo* in the most clinically
532 relevant preclinical model, the NHPs. Cynomolgus monkeys (*Macaca fascicularis*) were used
533 as they exhibit high resemblance with human anatomy and physiology, this NHP species is the
534 most frequently used in toxicology studies, including AAV9 gene therapy studies (45,54). In
535 order to closely mimic the intended clinical protocol, juvenile animals were injected with
536 Urbagen by bilateral ICV administration at 3.15×10^{13} vg/NHP or 7.85×10^{13} vg/NHP. As
537 several publications (44,55,56) suggest higher CNS transduction via intracisterna magna (ICM)
538 injection, a separate control group of animals received Urbagen at dose 3.15×10^{13} vg/NHP via
539 ICM delivery route. During the 90-day study, animals body weights and vital parameters
540 (breathing, heart rate, body temperature) were monitored daily. Gross motor functions and
541 reflexes were checked on a weekly basis. Blood analysis and histopathology assessment of
542 possible vector toxicity in various organs, including brain, liver, heart, DRGs, spleen, gonads,
543 etc. were performed at the end of the study. Finally, the biodistribution pattern of Urbagen was
544 determined using tissues harvested at study termination (Fig. 6a).

545 Body weight analysis throughout the study confirmed that all treated animals gained body
546 weight throughout the study as expected based on the age of the animals. CNS activity was
547 also unchanged, as normal reflexes were observed in all animals (Supplementary Fig. 19a-b).
548 Blood coagulation tests confirmed no influence of Urbagen on hematological status of the
549 animals as the APTT and the international normalized ratio (INR) values were similar in all
550 tested subjects (Supplementary Fig. 19c-d) and in the range with the reported values in
551 cynomolgus monkeys (57).

552 Complete blood count with differential revealed that Urbagen did not cause inflammation,
553 allergic reactions or other side effects as values of neutrophils, lymphocytes, eosinophils were
554 within normal reference ranges. Hemoglobin, hematocrit and red blood cell indices, as well as
555 platelet counts, were within normal ranges, indicating no evidence of coagulopathy or impaired
556 erythropoiesis (Supplementary Fig. 20). In addition, clinical biochemistry confirmed the safety
557 of Urbagen. AAV9-based therapies can cause several systemic toxic effects, where
558 hepatotoxicity and DRG toxicity are the most prominent and life-threatening events
559 (33,46,53,54). Blood panel analysis revealed that values of liver enzymes, such as ALT, AST,

and ALP, as well as urea, creatine kinase and other metabolites were all within normal physiological ranges, confirming that Urbagen does not cause systemic toxic effects (Fig. 6b, Supplementary Fig. 21).

Necropsy showing no macroscopic morphological changes in any treated animal. Furthermore, histopathology assessment based on scoring of H&E-stained tissue sections showed no DRG toxicity (Fig. 6c). Brain structures were preserved in all animals with no observable pathology (Supplementary Fig. 22). The frontal pole showed focal mononuclear cells near the lateral fissure. The anterior commissure contained brown pigmentation in the optical chiasm, similar to the lungs. Furthermore, liver, lungs and heart exhibited minor focal inflammatory cell infiltration (Supplementary Fig. 23, Supplementary Table 14).

Vector DNA and *hCTNNB1* mRNA biodistribution data obtained 90 days after vector administration revealed that the vector was widely distributed throughout different parts of the brain. ICM delivery route resulted in lower overall vector DNA levels compared to ICV injection, except in the pons, where the ICM-treated animals exhibited slightly higher values compared to the ICV injection groups (Fig. 6d). High vector DNA levels were also present in the spinal cord and across all DRG segments. In contrast, among peripheral tissue, only liver and spleen showed vector DNA levels above the LOD, while lungs, heart and gonads exhibited levels below the detection limit (Fig. 6e). Analysis of *hCTNNB1* mRNA normalized to *Macaca fascicularis* GAPDH expression suggest that the transgene is mostly expressed in cortex, cerebellum and in gyri (Fig. 6f). Detectable transcript levels were also observed in the spinal cord, cervical and thoracic DRG, whereas lumbar DRG lacked detectable *hCTNNB1* mRNA expression. In peripheral organs, transgene expression remained below LOD, with only minimal to absent expression detected in the liver, lungs, spleen, and gonads (Fig. 6g).

Discussion

This study presents preclinical development of the first AAV9-based gene therapy for CTNNB1 Syndrome, a severe and progressive neurodevelopmental disorder caused by β-catenin haploinsufficiency (2). Through systematic evaluation in patient-derived cortical brain organoids, a CTNNB1 Syndrome mouse model, and comprehensive toxicology and biodistribution studies in mice and NHPs, we demonstrated that AAV9-CTNNB1(C4) can

590 safely restore β-catenin expression, ameliorate disease phenotypes and support clinical
591 translation.

592 Among six AAV-CTNNB1 constructs tested, construct AAV-CTNNB1(C4) emerged as the
593 lead candidate, demonstrating the ability to restore *CTNNB1* mRNA to physiological levels in
594 patient-derived cortical brain organoids. This selectivity among constructs carrying similar
595 transgene cargoes but differing in regulatory architecture underscores the critical influence of
596 construct design on transcriptional output, and thus safety and potential clinical efficacy of
597 experimental gene therapeutics. The superior performance of construct AAV-CTNNB1(C4)
598 likely reflects the positive regulatory effects that intronic sequences can exert over transgene
599 expression. Some introns can enhance gene expression through a phenomenon called intron-
600 mediated enhancement (IME), whereby intronic sequences harbor transcription factor binding
601 sites or other regulatory elements that promote transcription (58,59). Beyond transcriptional
602 effects, the act of splicing itself can enhance transcript stability, as is well documented for other
603 genes, for example human β-globin (60). During spliceosome-mediated intron removal, the
604 exon junction complex (EJC) binds to the mRNA, promoting nuclear mRNA export efficiency,
605 and protecting it from nonsense-mediated decay (61).

606 The transcriptomic findings derived from patient organoids were interpreted as supportive
607 mechanistic evidence. Within this conservative framework, AAV2.7m8-CTNNB1(C4)
608 treatment was associated with directional changes in pathways linked to cell adhesion, synaptic
609 function and neuronal maturation, consistent with partial restoration of β-catenin-dependent
610 cellular processes. Consistent with this interpretation, pathway-level analyses identified
611 transcriptional shifts that were biologically concordant with restored β-catenin function. Genes
612 involved in cell-cell junction organization and focal adhesion showed directional increases
613 after treatment, in keeping with the established structural role of β-catenin at adherent junctions
614 (17). In parallel, genes associated with glutamatergic synapse pathways were also increased,
615 consistent with the known roles of β-catenin in synaptic vesicle organization and postsynaptic
616 scaffolding (13). Although these pathway-level changes should be interpreted cautiously in
617 light of organoid heterogeneity and limited sample size, their overall directionality supports a
618 model in which AAV-CTNNB1(C4) promotes partial restoration of neuronal stabilization and
619 maturation programmes without evidence of aberrant proliferative or oncogenic transcriptional
620 activation. The superior performance of AAV-CTNNB1(C4) in organoids was further
621 supported at the protein level. Treatment normalized β-catenin expression and was

accompanied by recovery of synaptophysin and GFAP, supporting partial restoration of disease-relevant neuronal and astrocytic phenotypes. These findings are notable given the established roles of β-catenin in synapse formation and plasticity (10), as well as in astrocyte biology (34), both of which are central to normal neurodevelopment and circuit function. Given the well-established role of aberrant Wnt/β-catenin signaling in tumorigenesis (37), oncogenic safety was further assessed by RNA-seq in treated patient-derived organoids. Importantly, no evidence of oncogenic promotion was detected. Pathway-level analyses of E2F targets, G2M checkpoint, MYC targets, p53 signaling and canonical Wnt/β-catenin signaling showed no aberrant activation after treatment, and Wnt/β-catenin pathway activity remained at or below the range observed in wild-type organoids. Together, these data support a favorable transcriptional safety profile for AAV-CTNNB1(C4), which was subsequently examined further *in vivo*.

The developed β-catenin$^{+/-}$ mouse model, showing approximately 50% reduction in β-catenin protein levels in CNS and peripheral tissues, recapitulates key motor and behavioral features observed in CTNNB1 Syndrome patients, including locomotor deficits and anxiety-like behaviors, seen also in ASD patients (62). Treatment with AAV9-CTNNB1(C4) at 4-weeks of age resulted in dose-dependent improvements across multiple behavioral domains. Systemic intravenous delivery of AAVs has been widely used in clinical gene-therapy programs for CNS disorders, including clinical trials for Canavan disease (NCT04998396) and the approved therapy Zolgenzma (Onasemnogene Abeparvovec) (63) for Spinal Muscular Atrophy (SMA). However, because the blood-brain barrier (BBB) limits efficient vector entry into the CNS, systemic administration often requires very high vector doses to achieve meaningful CNS penetration. Furthermore, a substantial proportion of the administered vector is sequestered in peripheral tissues such as liver and heart before reaching the brain and spinal cord. These high systemic doses can increase the risk of off-target toxicities, induce peripheral immune responses or liver toxicity, both of which have been reported in clinical studies as well as in market approved gene therapies (64,65), and may exclude patients with preexisting neutralizing antibodies against the AAV capsid (66).

In contrast, direct CNS delivery routes, including intrathecal (IT), ICV, ICM and direct intraparenchymal administration, can offer several advantages. These include bypassing the BBB, reduction of the required therapeutic dose, improved delivery to the relevant disease cell populations and reduced systemic side effects, including lower systemic immune activation,

all of which have been observed in clinical trials for Giant Axonal Neuropathy (GAN) (67), Spastic Paraplegia 50 (SPG50) (45,68) and the approved therapy Upstaza/Kebilidi for Aromatic L-amino acid decarboxylase (AADC) deficiency (69). In the present study, direct ICV delivery was used in all animal experiments to maximize brain transduction efficiency and therapeutic potential. In the mouse efficacy study, high-dose-treated animals showed significantly increased rearing activity in the Open Field Test, consistent with improvement in anxiety-like behavior, a phenotype relevant to CTNNB1 Syndrome. Kinematic gait analysis revealed specific motor improvements in treated mice, including normalization of back posture (tail base, iliac crest, and hip height positions), joint angles, stride time and movement trajectories during the swing phase, suggesting that treatment with Urbagen may positively influence motor impairments in CTNNB1 Syndrome patients. These improvements were dose-dependent and sex-specific, with females showing enhanced overall gait scores at 12 weeks of age and males at 20 weeks of age. The delayed response in males may reflect sex-specific developmental trajectories or differences in AAV transduction efficiency (70), a phenomenon that warrants further investigation.

It is noteworthy that genotype dependent change in body weight was not fully corrected in the murine model by the treatment, suggesting that some aspects of the CTNNB1 phenotype may be less amenable to intervention at this developmental stage or may require sustained elevated levels of β-catenin expression. However, the improvements in motor function and anxiety-like behavior indicate that therapeutic benefit can be achieved in key functional domains even without complete phenotypic rescue. Importantly, molecular analyses confirmed dose-dependent increases in both *CTNNB1* mRNA and β-catenin protein levels across multiple brain regions in treated animals, with no detectable increase in peripheral tissues such as liver and muscle, validating the CNS-selective expression profile and safety of the therapeutic vector. This was later confirmed by comprehensive blood biochemistry analyses that revealed no clinically meaningful changes compared with baseline or control animals.

Development of new experimental therapies requires extensive evaluation of safety and biodistribution *in vivo,* prior to first-in-human trials. These studies are essential for defining the potential risks and anticipated therapeutic window, thereby informing the overall risk-benefit assessment before human administration. Toxicology studies help establish the safety profile of the product, whereas biodistribution studies assess how the vector distributes throughout the body, including to tissues and organs outside the intended target site (71).

Urbagen was therefore evaluated in GLP, GLP-like and non-GLP toxicology and biodistribution studies conducted in accordance with harmonized national regulatory guidelines (48–52). The 8-month non-GLP toxicology study in wild-type mice provided important evidence of long-term safety. No adverse effects on growth, behavior, or survival rate were observed in animals receiving up to 2.25×10^{11} vg of AAV9-CTNNB1(C4). Biochemical markers of liver and kidney function remained within normal ranges throughout the study, and histopathological examination revealed no treatment-related abnormalities. The sporadic observations of neuronal degeneration and vacuolation in brain tissue were attributed to tissue processing artifacts rather than treatment-induced toxicity, as these findings occurred at similar frequencies across untreated and treated groups.

Toxicology and biodistribution studies using the GMP-like vector preparation, Urbagen, were designed to provide robust safety data to support first in human clinical translation in accordance with the EMA ICH S12 guideline. Most animals across all groups remained in normal clinical condition (score 0) throughout the study, as further supported by comprehensive blood and urine analyses. Observed findings were mild and included localized coat changes (e.g. barbering, alopecia, minor scabs, consistent with inter-male aggression), occasional corneal opacity, and rare transient signs such as increased respiratory rate or hypoactivity. These findings occurred sporadically across all groups, including controls, without a dose-response relationship. No treatment-related adverse clinical signs or mortality were identified, and all observations were consistent with background strain characteristics or housing-related effects in C57BL/6N mice. No treatment-related ocular abnormalities or signs of toxicity were noted during ophthalmological examinations conducted at study termination. High-grade inflammatory infiltration was observed in some high-dose-treated animals, often accompanied by asymmetrical ventriculi and localized neuronal degeneration. These findings were consistent with previously reported effects of high-dose CNS-administered AAV vectors (72) and were thought to reflect immune responses to high vector loads or transgene expression. Importantly, these inflammatory responses were localized, showed no evidence of widespread tissue destruction, and were considered clinically manageable through corticosteroid prophylaxis, which became a standard practice in AAV gene therapy trials (73).

Two male animals from the medium dose group in the 90-day GLP toxicology study met predefined humane endpoint criteria and were euthanized prior to scheduled necropsy. Both animals exhibited marked hydrocephalus with asymmetric brain morphology and enlarged

cranial cavity. One animal developed acute weight loss, labored respiration, tremors, and severe hypoactivity on study day 26. The second exhibited progressive decline culminating in >20% weight loss, neurological impairment, and marked hypoactivity by study day 47. The two humane endpoint cases were isolated to the mid-dose group, with no similar findings in other groups, including the high-dose group. The absence of a dose–response relationship suggests that these events were likely idiosyncratic. Several additional observations support the interpretation that these lesions reflected genetic anomalies rather than vector-related toxicity. The lesions occurred only in littermates, suggesting a heritable mutation, and no similar findings were detected in 78 additional animals across all other groups and studies. This interpretation is further supported by published reports of comparable spontaneous lesions in C57BL/6J, albeit at low incidence, related to genetic background (74).

Across all biodistribution studies, including the 28-day, 90-day and 180-day studies, no animals became moribund or exhibited signs of pain or distress, and all survived to scheduled necropsy. Biodistribution studies revealed highest vector DNA levels in the hippocampus and at the injection site in a dose-dependent manner, with significant presence also detected in the liver. Pro-vector DNA persisted in all tested CNS tissues at the 3- and 6-month timepoints, as well as in the liver. Detectable vector levels declined over time, particularly in blood, feces and peripheral tissues such as gonads, heart and kidney, indicating progressive vector clearance from off-target cells while maintaining stable levels in the CNS. Consistent with this, transgene mRNA expression profile was maintained in the cortex at 3 and 6 months, confirming sustained therapeutic gene expression in the target tissue.

The 90-day non-GLP study in cynomolgus monkeys provided critical translational data. Animals receiving Urbagen via either ICV or ICM routes showed no treatment-related adverse effects. Body weight, reflexes, and hematological parameters, including coagulation markers, remained normal throughout the study. Clinical biochemistry revealed no evidence of hepatotoxicity or systemic inflammation, with liver enzymes and other metabolic markers remaining within accepted physiological ranges (75).

Histopathological assessment confirmed complete absence of DRG toxicity, a critical finding given the documented susceptibility of primate DRGs to AAV9-mediated toxicity at high doses (76,77). Minor, low-grade changes were observed in some tissues, including focal mononuclear cells in frontal pole, pigment deposition in anterior commissure and lungs, minor inflammatory

infiltration in liver, lungs, and heart, but these were not dose-dependent and were considered incidental findings consistent with the age and handling of the animals.

Biodistribution analysis revealed widespread vector distribution throughout the brain following both ICV and ICM administrations, with ICM administration resulting in lower overall CNS vector levels except in the pons. The results suggest lack of dose dependence at the vector doses tested following ICV delivery, which can be at least partially attributed to the low number of animals per group. Nevertheless, both delivery routes achieved robust transduction of the spinal cord and DRG segments. Peripheral biodistribution was primarily limited to the liver and spleen, with minimal vector DNA in the lungs and heart, while levels in other tissues were below the limit of detection. Importantly, *hCTNNB1* transgene expression was predominantly detected in cortex, gyri, and cervical DRG with minimal or absent expression in peripheral organs.

The differential pattern between vector DNA presence and transgene mRNA expression in the NHP liver supports the ability of miR122a-5p and miR199a-5p to limit transgene expression in this tissue. However, although inclusion of miR183-5p targeting sequences clearly reduced dorsal root ganglion expression in the FRG mouse model, complete elimination of transgene expression in the dorsal root ganglia was not achieved in subsequent mouse and NHP studies. This may be related to the fact that liver miRTS-based detargeting was driven by two of the incorporated target sites, miR122a-5p and miR199a-5p, while only one, miR183-5p, was included for dorsal root ganglia de-targeting. These data likely reflect the inherent challenges of achieving complete silencing through miRNA-mediated mechanisms when vector loads are high. Similar effects have been reported in several previous studies, where high systemic doses increased the risk of off-target toxicities, including peripheral immune responses and liver toxicity, adverse events that have also been observed in clinical studies as well as in market approved gene therapies. Additional silencing strategies, such as increasing the number of target binding sites, or optimizing their placement to address possible secondary structure-proximity issues, could further improve the observed outcomes. Alternative or complementary de-targeting strategies, such as capsid engineering to reduce DRG tropism (78,79), may warrant consideration in future vector iterations. However, the absence of DRG and liver toxicity in our NHP study confirms that Urbagen cassette provides sufficient protection from off-target toxicity.

Together, these findings support the safety and therapeutic potential of AAV9-CTNNB1(C4) (Urbagen) gene therapy, the first therapy for CTNNB1 Syndrome, a progressive neurodevelopmental disorder currently lacking a disease-modifying treatment. The improvements observed in motor function and anxiety-related behaviors in the mouse model, together with the favorable safety profile observed across species, provided the foundation for a Phase I/II clinical trial initiated in Europe in December 2025 (NCT07270549).

Methods

AAV Plasmid design

Six versions of therapeutic cassette encoding *CTNNB1* coding region were designed and cloned. These plasmids contained the unmodified *CTNNB1* coding sequence (CDS), codon optimized (COP), or truncated (ΔCTD) variants, under the control of the cytomegalovirus enhancer/chicken β-actin hybrid (CBh) promoter and the bovine growth hormone (bGH) polyadenylation signal (pA). One of the cassettes included the polyadenylation signal endogenous to *CTNNB1* (3'UTR). Between the *CTNNB1* CDS and the pA, a mix of miRNA targeting sequences (miRTS) was incorporated in all constructs to prevent the expression of the transgene in the liver and DRG. Moreover, some of the plasmids included additional regulatory elements located in the *CTNNB1* gene, such as fragments of the 5'UTR or the introns.

Research-grade AAV production

For *in vitro* experiments, each AAV-CTNNB1 expression cassette, as well as the AAV-eGFP control, were individually packaged in AAV2.7m8 capsids using a standard helper-virus-free transient transfection-based system, whereas only the AAV-CTNNB1(C4) and AAV-eGFP cassettes were packaged into AAV9 capsids for *in vivo* experiments. Specifically, for each production, ten 15 cm dishes of adherent human embryonic kidney HEK293T cells were subjected to triple co-transfection using polyethylenimine (PEI; Bio Scientific, cat# 24765) with a 1:1:2 molar ratio of pRep2Cap : pTransgene : pAd5 at PEI:DNA ratio of 2:1. Mix contained DNA and PEI complexes was formed in OptiMEM (Gibco™, Cat# 31985) medium,

incubated for 10 min at room temperature, and added dropwise to the cells. Three days post-transfection, cells and culture media were separately harvested, and the AAVs were purified by iodixanol gradient (Sigma-Aldrich, cat# D1556) as previously described (80). Briefly, cell lysates were subjected to ultracentrifugation at 58,000 RPM for 2 hours at 18 ºC (Beckman Coulter rotor 70Ti, cat# 337922), after which the fraction containing the vector was isolated and subjected to buffer exchange and concentration. Buffer exchange (phosphate-buffered saline [PBS; Gibco, cat# 14190], 50 mM NaCl [Sigma-Aldrich, cat# S5150], 0.001%, Pluronic F68 [v/v; Gibco cat# 24040]) and concentration step were performed using Amicon Ultra-4 Centrifuge Filter Units (EMD Millipore, cat# UFC910096). The resulting AAVs were diluted and titrated using ddPCR and primers for the bovine growth hormone gene poly A signal (For: 5'GCCTTCCTTGACCCTGGA; Rev: 5'ACTCAGACAATGCGATGCAA) or the promoter (For: 5'ACGCCAATAGGGACTTTCCA; Rev: 5'GGGCGTACTTGGCATATGAT).

For *in vivo* experiments, the AAV-CTNNB1(4) expression cassette was packaged into AAV9 capsids by triple co-transfection and subsequent purification using double Cesium Chloride (CsCl, Sigma-Aldrich, cat# 562599) gradient ultracentrifugation as previously described (81).

Validation of miRTS in humanized FRG mice

All animal experiments were performed in accordance with institutional and national guidelines for the care and use of laboratory animals, under an approved animal ethics protocol (Protocol No. C389). Female *Fah*$^{-/-}$/*Rag2*$^{-/-}$/*Il2rg*$^{-/-}$ mice were bred at CMRI and maintained, engrafted and monitored as previously described (82). Mice were maintained in individually ventilated cages (IVCs) and provided drinking water supplemented with (2-(2-nitro-4-trifluoromethylbenzoyl)-1,3-cyclohexanedione) (NTBC, Yecuris, cat# 20-0028). At 6-8 weeks of age, FRG mice were engrafted with human hepatocytes (Lonza, cat# HUM181971) as previously described (82). The extent of human hepatocyte engraftment was determined by measuring circulating human albumin using a quantitative ELISA assay (Bethyl Laboratories, cat# E80-129). AAV9-eGFP vector administration was carried out via lateral tail vein infusion at a dose of 2.00×10^{11} or 4.00×10^{12} vg/mouse, and animals were kept on 10% NTBC throughout the study period until the time of tissue collection four weeks post vector administration. Liver tissue and DRGs were harvested and fixed in 4% paraformaldehyde (PFA, Scharlau, cat# PA0950500) for 24 hours. Liver samples were subsequently embedded

in optimal cutting temperature (OCT) compound and cryosectioned at 5 µm using the Leica CM1950 cryostat prior to counterstaining with DAPI. Whole-mount DRGs were directly stained and imaged for GFP signal detection using a fluorescence microscope (ZEISS Axio Imager.Z2) with the same exposure settings for all sections.

Generation of *CTNNB1-KO* HEK293T cells

Single-stranded oligonucleotides encoding guide RNAs (gRNAs) targeting exon 3 (CAACAGTCTTACCTGGACTC) and exon 13 (GCATATGTCGCTAAGAGACA) of *CTNNB1* were designed using the CRISPOR web tool (83), synthesized by Macrogen and prepared for cloning through annealing and phosphorylation. The resulting duplexes were ligated into the BbsI site of the pSpCas9(BB)-2A-Puro vector (Addgene, cat# 62988) and verified by Sanger sequencing. HEK293T cells were transfected with the gRNA-Cas9 constructs using Lipofectamine 3000 (Thermo Fisher Scientific, cat# L3000015) following the manufacturer's protocol. Twenty-four hours post-transfection, cells were subjected to puromycin selection (1 µg/mL) (Thermo Fisher Scientific, cat# A1113803) for 48 hours and subsequently expanded. Clonal populations were obtained by limiting dilution into 96-well plates, and successful knockout clones were identified by loss of β-catenin protein expression as determined by western blot analysis.

Functional validation of AAV-CTNNB1 cassettes in *CTNNB1-KO* HEK293 cells

In-house generated *CTNNB1*-KO HEK293 cells were seeded at a density of 3.75×10^5 cells per well in 24-well plates (Falcon®, cat# 353047). Four hours after seeding, cells were transduced with individual AAV9-CNNTB1 vectors at a dose of 2.00×10^6 vg/cell. Culture medium was replaced 16 hours post-transduction, and cells were harvested 96 hours post-transduction for DNA, RNA, and protein analyses. DNA and RNA were extracted using the Qiagen AllPrep DNA/RNA Mini Kit (Qiagen, cat# 80204) according to the manufacturer's instructions. RNA samples were treated with TURBO DNAse (Invitrogen, cat# AM2238) to remove genomic DNA, and cDNA was synthesized using the SuperScript™ IV First-Strand Synthesis System (Invitrogen, cat# 18091200). RT-qPCR was performed employing the iTaq™ Universal SYBR® Green Supermix (Bio-Rad, cat# 172-5121) with the following

primers at 10 µM: *GAPDH* For: 5'TGTTCGACAGTCAGCCGCATCTTC, Rev: 5'CAGAGTTAAAAGCAGCCCTGGTGA; *CTNNB1* For: 5'CTAGTTCAGTTGCTTGTTCGTG, Rev: 5'CCTTCAACTATTTCTTCCATGCG. Data are shown as fold change (mean ± SEM) relative to the wild-type, calculated using the $2^{-\Delta\Delta Ct}$ (Livak) method. Statistical comparisons were performed on $-\Delta\Delta Ct$, using one-way ANOVA and Fisher's Least Significant Difference (LSD) multiple comparisons test against the WT group.

Proteins were extracted using lysis buffer containing RIPA buffer (Thermo Fisher Scientific, cat# 89901) and Halt (Thermo Fisher Scientific, cat# 78441), and quantified using Pierce™ BCA Protein Assay Kit (Pierce, cat# 23225) as per manufacturer's instructions. Western blot was performed under denaturing conditions using the blocking buffers and dilutions specified by the antibody supplier (β-catenin: Abcam, cat# ab32572, lot# 1038258-64, 1:1000; GAPDH: Cell Signaling, cat# 2118, lot# 16, 1:2,500). Chemiluminescent signal was detected using the ECL substrate (Amersham, cat# RPN2209) and ChemiDoc Imaging System (Bio-Rad) and semi-quantified with FIJI normalizing β-catenin protein signal against GAPDH protein. Comparison between groups was performed using ANOVA as parametric test (Shapiro Wilk > 0.05) and Dunnett's multiple comparisons test.

Organoid experiments

Organoids were generated from iPSCs derived from a patient with CTNNB1 Syndrome in the Stem Cell and Organoid Facility at Children's Medical Research Institute (CMRI).

For the generation of iPSCs, viable Peripheral Blood Mononuclear cells (PBMCs) were recovered from anticoagulated blood via density gradient centrifugation with Histopaque-1077 (Merck, cat# 10771) at 500 g for 30 minutes. Recovered fraction containing PBMCs was then washed twice with 1×D-PBS and centrifuged at 300 g for 30 and 10 minutes respectively. Isolated PBMCs were then resuspended in frozen media containing 90% Knockout Serum Replacement (Thermo Fisher Scientific, cat# 10828028) and 10% DMSO (Merck, cat# D2650).

PBMCs were cultured for six days in Expansion media consisting of STEMSPAN H3000 (StemCell Technologies, cat# 9850) supplemented with 50 µg/mL Ascorbic acid (Merck, cat#

A4544-25G), 50 ng/mL SCF (Miltenyi, cat# 130-096-692), 10 ng/mL IL-3 (Thermo Fisher Scientific, cat# PHC0035), 2 U/mL EPO (R&D, cat# 287-TC-500), 40 ng/mL IGF-1 (Miltenyi, cat# 130-093-885) and 1 μM Dexamethasone (Merck, cat# D8893-1MG). On day 6, 2×10^5 PBMCs were nucleofected with 0.33 μg of the episomal plasmids pCXLE-hUL (Addgene, cat# 27080), pCXLE-hSK (Addgene, cat# 27078) and pCXLE-hOCT3/4-shp53-F (Addgene, cat# 27077) using the P3 Primary Cell 4D-Nucleofector X kit L (Lonza, cat# V4XP-3024) and the program EO-115 of the Amaxa 4D system (Lonza). Nucleofected cells were then plated on a Geltrex-coated single well of a 6-well plate and fed daily with Essential 8 media (Thermo Fisher Scientific, cat# A1517001). Emerging colonies were observed and picked around 2-weeks post-nucleofection and cultured for 10 passages prior to characterization by karyotyping and immunofluorescence staining for pluripotency markers LIN28, SOX2, NANOG and OCT4.

The iPSCs were differentiated into cortical brain organoids using a protocol adapted from Yoon and Pasca (84) with some modifications. Briefly, human iPSCs were grown to 70-80% confluence in stem cell media consisting of Essential 8 (E8, Thermo Fisher Scientific, cat# A1517001) and incubated with 1% DMSO (Merck, cat# D2650) for 24 hours (Day -1). Human iPSCs were additionally incubated in stem cell media containing both 1% DMSO and 10 μM ROCK inhibitor (StemCell Technologies, cat# 72304) one-hour prior single cell dissociation (Day 0) followed by dissociation using StemPro Accutase (Thermo Fisher Scientific, cat# A1110501). Cells were pelleted, counted and seeded in low binding Nunclon Sphera 96-well U-bottom plates (Thermo Fisher Scientific, cat# 174925) at a concentration of 10,000 cells per 100 μL in E8 media with 10 μM of ROCK inhibitor per well. On day 1, additional 100 μL of E8 media without ROCK inhibitor per well were added. From day 2, media was replaced with Essential 6 (Thermo Fisher Scientific, cat# A1516401) containing 2.5 μM Dorsomorphin (Merck, cat# P5499-5MG) and 10 μM SB431542 (Tocris, cat# 1614). On day 7, organoids were transferred to a 6-well plate in a rocker shaker (85 RPM) and fed daily with NM basal media containing 20 ng/mL EGF (R&D, cat #236-EG-200) and 20 ng/mL FGF2 (R&D, cat# 233-FB-025) for the next 10 days, and every other day until day 26. Media was then changed to NM containing 20 ng/mL NT3 (Peprotech, cat# 450-03-50UG) and 20 ng/mL BDNF (Peprotech, cat# 450-02-50UG) and organoids fed every other day until Day 44. From there onwards, organoids are fed with NM alone. The composition of NM basal media is Neurobasal – A (Thermo Fisher Scientific, cat# 10888022) supplemented with B27 supplement minus Vitamin A (Thermo Fisher Scientific, cat# 12587001), Glutamax (Thermo Fisher Scientific,

cat# 35050079), Penicillin-Streptomycin (Thermo Fisher Scientific, cat# 15140122) and Amphotericin B (Thermo Fisher Scientific, cat# 15290026).

Cortical brain organoids were transduced with 1.00×10^{10} vg/organoid at two developmental timepoints, termed T1 and T2. T1 samples were transduced at differentiation day 23 and collected at day 37, whereas T2 samples were transduced at day 43 and collected at day 57, for immunofluorescence and mRNA analyses. Healthy donor-derived cortical organoids, untreated patient-derived organoids and organoids treated with an AAV2.7m8-eGFP control vector were used as controls.

RNA was extracted using Qiagen AllPrep DNA/RNA Mini kit (Qiagen, cat# 80204) as per manufacturer's instructions. RNA was then employed for RT-qPCR as described above or for RNA-sequencing.

For immunofluorescence analysis, organoids were fixed in 4% PFA for one hour, washed in 1×D-PBS and transferred to 20% sucrose. Subsequently, organoids were embedded in OCT (ProSciTech, cat# IA018) and sections were cut at 14 µm. Immunodetection was performed using antibodies targeting LIN28 (Cell Signaling, cat# 3695, lot# 2, 1:400), SOX2 (Cell Signaling, cat# 3579, lot# 8, 1:400), NANOG (Cell Signaling, cat# 4903, lot# 8, 1:200), OCT4 (Cell Signaling, cat# 2840, lot# 20, 1:400), β-catenin (Abcam, cat# ab32572, lot# 1038258-63, 1:200), synaptophysin (Abcam, cat# ab8049, lot# 1096179-1, 1:200), and GFAP (Agilent Technologies, cat# Z0334, lot# 41526076, 1:200), and employing anti-rabbit (Invitrogen, cat# A32754, lot# WD319534, 1:500) and anti-mouse (Invitrogen, cat# A31571, lot# 2045337, 1:500) as secondary antibodies. Slides were imaged at 20× and 40× magnification with the fluorescence microscope (ZEISS Axio Imager.Z2) with identical exposure settings applied to all samples for each target. For semi-quantitative analysis of immunofluorescence images, histogram ranges were adjusted using the highest pixel intensity observed in any image of a given target to standardize the range of all other images using ZEN software. Fluorescence of the images was then quantified using FIJI, which generated a mask over the areas exceeding a defined threshold and measured the masked area.

At least three independent differentiation batches were generated across the organoid workflow. RT-qPCR and immunofluorescence data were analyzed across the biological replicates indicated for each experiment. Residual normality was assessed using the Shapiro-Wilk test. Where assumptions for parametric testing were satisfied, group comparisons were

performed using one-way ANOVA followed by Dunnett's multiple-comparisons test. A two-sided p value < 0.05 was considered statistically significant.

RNA sequencing data processing, normalization and Differential Gene Expression (DGE) analysis

Total RNA was extracted from cortical brain organoids (Sigma Aldrich, cat# RTN9604), and 2 µg per sample was submitted to GENEWIZ for bulk RNA sequencing at the two stablished developmental timepoints. Downstream bioinformatic analyses were performed in-house. Transcriptomic interpretation was restricted to datasets that met quality and consistency criteria, which showed the clearest internal clustering structure and most interpretable separation across conditions in exploratory analyses.

Raw sequencing reads were quality controlled using FastQC (v0.12.1) and aligned to the reference genome using HISAT2 (v2.2.1). Gene-level expression data were imported into R for downstream analysis. Following addition of a pseudocount, expression values were log2-transformed and normalized using the voom function in limma (v3.58.1). Differential expression analysis was performed using limma together with edgeR (v4.0.16), according to the experimental design. Linear models were fitted using lmFit and moderated using empirical Bayes shrinkage with eBayes. Principal component analysis (PCA) was used for quality assessment of sample clustering and to identify batch-associated structure in the dataset.

Functional enrichment analyses, including KEGG pathway and Gene Ontology analyses, were performed to identify biological processes associated with treatment. Gene set variation analysis was additionally used to assess pathway-level changes in oncogenic, proliferation-related, adhesion-related, synaptic and neuronal maturation programmes. Given the use of RNA-seq as a supportive mechanistic dataset within a heterogeneous and batch-variable organoid model, interpretation focused primarily on concordant pathway-level changes and biological coherence across orthogonal readouts, rather than on isolated single-gene differences.

Generation of a heterozygous *Ctnnb1* mouse model

For the efficacy study heterozygous *Ctnnb1* mice (*Ctnnb1* het; β-catenin$^{+/-}$, β-cat$^{+/-}$) were developed following IACUC approval at Jackson Laboratory. Beta-catenin$^{+/-}$ mice were generated by mating B6.129-*Ctnnb1*^{tm2Kem}/KnwJ (β-catenin^{flox}; strain code IMSR_JAX:004152)(36) and B6.Cg-*Edil3*$^{Tg(Sox2-cre)1Amc}$/J (Sox2Cre; strain code IMSR_JAX:008454)(37) mice. β-cat$^{+/-}$mice (Ctnnb1<tm2Kem>/KnwJ;Sox2Cre) are heterozygous for abolished gene segments from 1st to 6th intron of the *Ctnnb1* gene (MGI:2148567). Mating of β-catenin^{flox} and Sox2Cre resulted in Cre-hemizygous mice that carry a deletion of a single allele of the *Ctnnb1* gene. These animals were further crossed with C57BL/6J OlaHsd. From their offspring, the Cre-negative mice with a deleted *Ctnnb1* allele were selected for colony consolidation. Genotyping of the offspring was carried out by the DNA extraction using Phire Tissue Direct PCR Master Mix (Thermo Fisher Scientific, cat# F170S) as per vendor recommendations. Primers used in the study: *Ctnnb1* wt For: 5'TGACCTGATGGAGTTGGACA, Rev: 5'ATCTTCTTCCTCAGGGTTGC; *Ctnnb1* het For: 5'TCAGGAAAAACATTGGATTTGT, Rev: 5'TATCCAGCCCCTCCTCTCTG. Appropriate genotypes were determined by standard agarose gel electrophoresis.

Mice efficacy study

All animal experiments were performed according to the directives of the EU 2010/63 and Commission recommendation 2007/526/EC and were approved by the National Animal Experiment Board of Finland (Permit Numbers ESAVI/10985/2020; ESAVI/45122/2022). This study was performed according to appropriate methodologies and standard operating procedures (SOPs) at the testing facility with regularly performed internal audits by the CR DRS Finland Ethics Committee and Animal Welfare Body. The Study Protocol was reviewed by the Animal Welfare Team. CR DS Finland site in Kuopio is accredited by AAALAC International.

Laboratory animals were housed in Individually Ventilated (IVC) cages Type II Long Cages (Allentown Inc.), fed standard chow (Teklad Global 2016) and provided tap water ad libitum. The cages were enriched with plastic igloo, gnawing material (aspen sticks), nesting material, and tunnels used for handling. Mice were maintained in 12-12-hour dark-light cycle at approximately 40-60% relative humidity with 21.5±1.5°C of ambient temperature. All animals used in the study were healthy; veterinary care was provided throughout the study.

To test the therapeutic effect of AAV9-CTNNB(C4), female and male 3 weeks β-cat$^{+/-}$ and β-cat$^{+/+}$ mice were used. Mice were assigned to treatment groups based on pre-treatment body weight, ensuring there were no significant differences between the individual groups of mice of the same genotype. Female and male animals were randomized separately. The efficacy study involved a single intracerebroventricular (ICV) administration of AAV9-CTNNB1, followed by assessments of behavioral and cognitive outcomes. ICV delivery was performed at 28±3 days of age, and mice were monitored until 23 weeks of age, when they were humanely sacrificed and samples were harvested.

AAV9-CTNNB1(C4) or AAV9-eGFP (control) was injected, by stereotactic injection as in (85), into the right lateral ventricle (AP -0.5 mm, ML +1 mm, DV -1.75 mm) using a Hamilton syringe and an infusion system (Harvard Apparatus). Animals were injected either with 2.13×10^{10} AAV9-eGFP vg/mouse or with AAV9-CTNNB1(C4) at low (4.24×10^{9} vg/mouse), mid (2.12×10^{10} vg/mouse), or high ($1.06 \times {}^{11}$ vg/mouse) doses in total volume of 5 µl.

Body weight of the mice was measured twice weekly starting after weaning. Samples after collection were weighed, and fresh frozen in liquid nitrogen immediately after collection and stored at -80 °C.

Human *CTNNB1* mRNA copy numbers were determined in brain samples. RNA isolation was carried out using GenElute96 well Total RNA Purification Kit (Sigma Aldrich, cat# RTN9604) with subsequent RNA quantification (Quant-iTKit, ThermoFisher, cat# Q33140) and integrity testing via TapeStationan alysis (Agilent). Reverse transcription (25 ng of RNA) was performed using RT Kit (Qiagen, cat# 205311). qPCR was used to determine the expression levels of human *CTNNB1* gene (For: 5'TGACCTGATGGAGTTGGACA, Rev: 5'ATCTTCTTCCTCAGGGTTGC), using mouse *Gapdh* as a housekeeping gene (For: 5' CATCACTGCCACCCAGAAGACTG, Rev: 5' ATGCCAGTGAGCTTCCCGTTCAG).

Beta-catenin protein expression was analyzed by ELISA assay, using Human beta Catenin (Total) ELISA Kit, 96 Tests (Thermo Fisher Scientific, cat# KHO1211) according to manufacturer's instructions. Samples were lysed in 5x Passive Lysis Buffer (Promega, cat# E1941) and next centrifuged (13,400 RPM / 30min / 4 °C). Supernatant was diluted 1:5 and absorbance (450 nm with background measurement at 620 nm) was determined using Tecan microplate reader.

Complete biochemical blood profile was determined using VetScan ® Comprehensive Diagnostic Profile (Zoetis, cat# 51631000) rotor and analyzed on the biochemistry analyzer VetScan VS2 (Abaxis) according to the manufacturer's instructions.

Behavioral tests

Marble Burying Test was performed at 12 and 20 weeks of age during the light phase. Mice were brought to dimly illuminated experimental room for at least 1 h acclimation to the experimental room conditions prior to testing. A transparent polycarbonate test cage (30 × 18 × 19 cm) was filled with a 5-cm layer of the standard bedding, and 24 marbles (1.5 cm in diameter) were placed evenly next to the walls of a cage. During the test, each mouse was transferred from its housing cage to a test cage individually (one mouse per cage). After a 30-min period, the mouse was transferred back to its home cage. The number of marbles covered (at least 2/3 of marble area) was counted and the test cage was photographed. The bedding material was replaced between tests, and the marbles were cleaned,

Open Field Test was performed at 4 (pre-treatment), 12 and 20 weeks of age, during the light phase. Prior to the test, mice were allowed to habituate to the test room for at least 60 minutes. Activity chambers (Med Associates Inc, St Albans, VT, USA; 27 cm × 27 cm × 20 cm) equipped with infrared beams, were used in the test. The mouse was placed in the center of the chamber, and the behavior was recorded for 30 minutes in 5 minutes bins. Quantitative analysis was performed on the following five dependent measures: total locomotion, locomotion in the center of the open field, rearing rate in the center, total rearing frequency, and velocity. Mice were tested at low-stress conditions with light intensity lowered to approximately 10 – 30 lux of red light.

Fine Motor Kinematic Gait Analysis was performed at 12 and 20 weeks of age, during the light phase. Prior to the test, mice were allowed to habituate to the test room for at least 1 hour. Pre-defined points, including limb joints and tail, were marked on the body to aid the data analysis process. Mice were allowed to move along a corridor, and the movement of the mouse was captured from three different directions (from below and both sides) using a high-speed camera (300 fps). The captured movements of the marked body points were converted to data points representing the movements of the different points as coordinates in relation to the ground and the correlation of the movements captured from the three dimensions. Different gait patterns

and movements were analyzed using a custom-made automated analysis system. The analyzed parameters included general gait pattern parameters (stride time and speed, step width, stance and swing time during a stride, interlimb coordination); body posture and balance (toe clearance, iliac crest and hip height, hind limb protraction and retraction, tail position and movement); and fine motor skills (swing speed during a stride, jerk metric during swing phase, angle ranges and deviations of different joints, vertical and horizontal head movement). PCA was used to identify different gait features or PC scores (difference between wild-type and heterozygous controls). Orthogonality preserving Varimax rotation procedure was used.

Radial Arm Water Maze Test was performed at 12 weeks of age, over two consecutive days, during the light phase. Prior to the test, mice were allowed to habituate to the test room for at least 1 hour. Mice were divided into test groups of 3-4 mice in each, balanced for the treatments. A six-arm maze was submerged in a pool of water, and a platform was placed at the end of one of the arms, 1 cm below the water surface. The mouse was subjected to 15 trials per day for 2 days, with each trial starting from a different arm while the platform remained in the same position throughout the trials on both days. Using visual cues around the room, the mouse was expected to learn the position of the escape platform. On both days 1 and 2, a hidden platform was used. The duration of a trial was 60 seconds. If the mouse did not find the platform and climb on it within 60 seconds, the mouse was placed on the platform for 5 sec. After each trial the mouse was placed in a cage placed on a warming mat for the inter-trial interval, to expedite the drying of the fur and to keep the mouse warm. The latency to find the platform, and the number of errors (incorrect arm entries, i.e. entries to arms without the platform) was counted over the 60-second period for each trial. The latency and number of errors were averaged over three trials resulting in 10 blocks for the two-day test period.

Y-maze test was performed at 20 weeks of age, during the light phase. Prior to testing, mice were allowed to habituate to the dimly illuminated experimental room for at least 1 hour. For the initial training trial, the mouse was placed at the end of one arm of a large Y-maze designated “start arm” (arm length: 37.5 cm). The third arm of the maze was blocked off, allowing the mouse to explore two of the three arms freely (“start arm” and “familiar arm”) for 5 min. The “familiar arm” contained spatial cues mounted on the wall at the end of the arm. One hour later, the mouse was placed back into the maze in the “start arm” and was allowed to explore all three arms with the third arm unblocked (“novel arm”). The “novel arm” contained distinct cues mounted on the wall at the end of the arm. Each test session was video recorded

and the number of entries to each arm and the amount of time in each arm were calculated from the videos. Testing was performed under dim lighting, and the apparatus was cleaned with 70% ethanol between trials.

Rotarod Test was performed at 12 and 20 weeks of age, at each age point over three consecutive days, during the light phase. Prior to the test, mice were allowed to habituate to the test room for at least 1 hour. Each of the three test days started with a training trial of 5 minutes at 4 RPM on the rotarod apparatus (Med Associates Inc, St Albans, VT, USA). One hour later, mice were tested for 3 consecutive accelerating trials of 6 min each with the speed changing from 0 to 40 RPM over 360 seconds. The inter-trial intervals were at least 30 minutes. The latency to fall from the rod was recorded.

Paw Clasping Test was performed at 12 and 20 weeks of age. The mouse was taken from the home cage and placed on the wire lid of the cage. The mouse was then suspended by tail for 30 seconds. The clasping rate was scored from 0 to 2: score of 0 representing no clasping behavior, score of 1 was given if the hind paws touched each other for at least 1 second, and score of 2 was given when the hind paws touched each other for more than 5 seconds. Additionally, latency (in seconds) to first incidence of hind paws touching each other was recorded.

Contextual Fear Conditioning Test (41) was performed at 20 weeks of age, during the light phase. Prior to the test, mice were allowed to habituate to the test room for at least 1 hour. The training and testing were conducted on two consecutive days, using a Med Associates fear conditioning system (Med Associates, Fairfax, VA, USA). On day 1 the training consisted of placing a mouse in a chamber, with the house light on, and allowing exploration for 103 sec. Afterward an auditory cue (1700 Hz, 80 dB) was presented for 15 sec. A 2-sec foot shock (1.0 mA) was administered for the final 2 sec of the stimuli. This procedure was repeated three times with an inter-shock interval of 60 sec (thus, altogether 4 shocks), and the mouse was removed from the chamber 30 sec after the last shock. Approximately 20 hours after the training, the mouse was returned to the same chamber in which the training occurred. The house light in the chamber was on during the 5 min test, thus the conditions in the chamber were similar to day 1, during training. At the end of the 5 minutes context test, the mouse was returned to its home cage. The freezing behavior was recorded by a computerized camera tracking system.

A non-GLP long-term single-dose toxicity study in mice

An 8-month non-GLP toxicology study was performed in C57BL/6J mice at the Bioresource Facility of the Westmead Institute for Medical Research (WIMR), Australia. The main goal of the study was to identify potential short- and long-term safety concerns associated with AAV9-CTNNB1(C4) administration. Mice at postnatal day 28±3 of age were used. Mice were acclimated for 5 days before the starting the study, with health observations and body weight recording every two days. Mice were housed in an enriched-environment with filtered air system and provided with ad libitum water and food and 12-12-hour dark/light cycle. Cohorts of five males and five females received intracerebroventricular injections of 5 μL of either AAV9-CTNNB1(C4) or control AAV9-eGFP vector at doses of 1.06×10^{11} or 2.25×10^{11} vg/mouse. Additional naïve undosed mice served as controls.

Animals were monitored weekly for body weight, survival, and physical appearance, and clinical signs of adverse effects throughout the study. Blood samples were collected at one week, three months, and eight months post-administration and centrifuged for 20 minutes at 2,000 × g and 4 ºC to obtain the plasma. Plasma samples then were employed for biochemical assessment of hepatic and renal function (ALB, ALT, ALP, TP, TBIL, CRE) using biochemistry analyzer VetScan VS2 (Abaxis).

At study termination, mice were humanely euthanized and transcardially perfused with cold 1× Hank's Balanced Salt solution (HBSS) (Gibco, cat# 14175095). Tissues were harvested, fixed in 4% PFA for 24 hours, transferred to 70% ethanol, processed, embedded in paraffin, sectioned at 4 μm, and stained with H&E for histopathological evaluation by a certified histopathologist.

Comparison of body weight change and cerebral cortex thickness between treatment groups was performed considering normality of residual values (Shapiro–Wilk) and homogeneity of variance between groups (Bartlett's or Brown-Forsythe tests). Body weight comparisons were performed using two-way ANOVA or mixed-effects model with repeated measures. One-way ANOVA was used as parametric test and Kruskal- Wallis test as non-parametric method for cerebral cortex thickness comparisons. Statistical significance was set at $p < 0.05$.

Production of GMP-like grade AAV9-CTNNB1(C4) viral vector, Urbagen

For biodistribution and toxicology studies, the drug candidate, AAV9-CTNNB1(C4), was produced under cGMP-like conditions, including required quality control (QC) and release testing by contract development and manufacturing organization (CDMO) - Viralgen, Spain. The manufacturing protocols use are the property of Viralgen and due to their proprietary nature cannot be provided.

Identity of the Viral Proteins (VP) was confirmed by SDS-PAGE and western blot, using Urbagen and AAV9 empty capsids (AAV9ec; PROGEN Biotechnik GmbH, cat# 66V090) diluted to 5.00×10^9 vector genomes per well. The primary antibody against VP1/VP2/VP3 (PROGEN Biotechnik GmbH, cat# 690058S, lot# DOK2274-13) was diluted 1:100, and the secondary antibody m-IgG Fc BP-HRP (Santa Cruz Biotechnology Inc., cat# sc-525416, lot# D1323) was diluted 1:1,000. VP bands were visualized using the ChemiDoc™ Touch Imaging System (Bio-Rad Laboratories, Inc).

Genome identity was verified by isolating vector DNA with the GeneJET Viral DNA/RNA Purification Kit (Thermo Fisher Scientific, cat# K0821) and performing Sanger sequencing (Eurofins).

A 28- and 90-day single intracerebroventricular dose biodistribution and toxicity study in mice

A 90-day single dose toxicity and biodistribution study was performed under GLP-compliance (GLP-2024-03), whereas a 28-day study was executed under GLP-like conditions. For both studies, juvenile (28±3 days) C57BL/6NCrl female and male mice were used. Study was approved by the Institutional Animal Care and Use Committee (IACUC) and the Resort Professional Commission of the CAS for Approval of Projects of Experiments on Animals (Approved Protocol No. 5509/2024) and in accordance with ICH Guideline M3 (R2). Additional guidelines were also followed: Non-clinical Safety Studies for the Conduct of Human Clinical Trials and Marketing Authorization for Pharmaceuticals, Guideline on quality, non-clinical and clinical aspects of gene therapy medicinal products (EMA/CAT/80183/2014) (49), Guideline on quality, non-clinical and clinical requirements for investigational advanced therapy medicinal products in clinical trials – Scientific guideline (EMA/CAT/123573/2024)

(50), ICH S12 Guideline on nonclinical biodistribution considerations for gene therapy products (EMA/CHMP/ICH/318372/2021) (51), and OECD Guidelines for the Testing of Chemicals, Section 4; Test No. 408: Repeated Dose 90-Day Oral Toxicity Study in Rodents (52).

Laboratory animals were housed under specific-pathogen-free (SPF) barrier in IVC cages GM500 (Techniplast), fed standard chow (Altromin 1314 Forti, Altromin International) and water provided ad libitum. Diet and water quality, consumption, and deposition were monitored for all animals on a weekly basis. Diet consumption was calculated: $Diet\ consumption = \frac{Initial\ Weight - Final\ Weight}{Number\ of\ animals\ in\ the\ cage\ x\ Time\ Interval}$.

Mice were maintained in 12-12-hour dark-light cycle at approximately 40-60% relative humidity with 19-23 °C of ambient temperature. All animals used in the study were healthy and veterinary care was provided constantly at the test facility.

Mice were acclimated for a minimum of 5 days before the start of the treatment. During acclimation animals were observed once daily, and all observations were recorded. Samples were collected at day 28, day 90 and additionally at day 180 (to prolong the biodistribution monitoring) post-test item administration. Vector was administered ICV into the right ventricle (total volume ~5 µL/mouse; injection rate: 0.5 µL/min) using a stereotaxic robot with StereoDrive stereotaxic system (Neurostar) (AP -0.4, ML 1.0, DV 2.55). On each dosing day, one Hamilton Syringe 10 µL 701 RN without needle (Hamilton Company, cat# 7635-01), a Hamilton RN Needle (30/12.7/PST4)S 6/PK (Hamilton Company, cat# 7803-17) and a drill bit TC cavity Burs Round 0.8 mm diameter (Dentsply Sirona, cat# DENT-E020524100810) were used. Test Item was administered in 3 different doses (5.00×10^{10} vg/mouse - low dose, 1.00×10^{11} vg/mouse - mid dose and 3.35×10^{11} vg/mouse - high dose). Control animals were administered the vehicle in the same manner (n=10 males and females for each dose group).

Once prior to administration and at least once a week thereafter, detailed clinical observation was performed on all animals. These observations were performed outside the cage in the standard arena and preferably at the same time. Detailed clinical observation was recorded using scoring system. All clinical signs and observations were scored (Supplementary Table 2).

All animals were individually weighed (Portable balance PS 3500.X2.M (RADWAG); Portable balance KERN EMB (KERN)) at delivery, before dosing, then weekly and before necropsy. Body weight change was calculated as follows: $Body\ weight\ change = \frac{Final\ Weight - Initial\ Weight}{First\ Weight}\ x\ 100$.

Animals underwent ophthalmological examinations (Direct ophthalmoscope BETA200 with LED): examination of the cornea, area of opacity, iris, conjunctivae, lacrimation, and chemosis (Supplementary Table 3).

Blood collection was performed on day 57 and at the end of the study from the retro-orbital sinus. Hematology analysis (reference values: Supplementary Table 3) (Mindray BC5300 Vet, Mindray) was conducted on whole blood samples collected in EDTA tubes (EDTA 1000 A tubes, KABE LABORTECHNIK GmbH, cat# 078001). Clinical chemistry analysis (reference values: Supplementary Table 5) (Beckman Coulter AU480, Beckman Coulter) was performed on Li-Heparin plasma samples (Li 1000 A Standard tube, KABE LABORTECHNIK GmbH). Coagulation analysis was performed on analyzer Sysmex CA-560 system (Sysmex Corporation). Urine and feces were collected overnight (16 hours) from animals housed in metabolic cages (Metabolic cages for mice with double chambre feeder, Tecniplast®, 3700M022). Urinalysis was performed on CLINITEK Advantus Urine Chemistry Analyzer by using reagent strips.

All euthanized animals (due to reached human endpoint or scheduled necropsy) were subjected to gross necropsy. All gross pathological changes were recorded including any findings on individual tissues and organs if present. Tissues for further histopathological analysis based on scoring (Supplementary Table 6) were collected. All collected tissues, except for the eyes with optic nerves and brain, were fixed in 4% neutral buffered formaldehyde (FA, prepared in house) for 24 hours immediately after collection during necropsy. Eyes with optic nerves and the brain were fixed in Davidson's fixative for 24 hours. After 24 hours of fixation all samples were trimmed, except bones and spinal cord, and were transferred to 70% ethanol. Bones and spinal cords were subjected to decalcification using Osteosoft® solution. Fixed samples in 70% ethanol were stored at +4°C until further processing. Tissue samples in histology cassettes were processed on Leica ASP6025 automatic vacuum tissue processor and embedded in paraffin in Leica EG1150 H+C embedding station (Leica Biosystems). Paraffin blocks were sectioned using a Leica RM2255 rotary microtome at a nominal thickness of 2 µm sections. Prepared

slides were stained with hematoxylin–eosin and mounted using Leica ST5020 automated staining instrument (Leica) in combination with the Leica CV5030 Glass Coverslipper (Leica Biosystems).

For biodistribution analysis, tissue samples were collected on ice by an RNase free method. For sample collection from the injection site, a sterile 2 mm biopsy punch (Kai Industries co.) was used to ensure precise sampling. All collected tissue samples were placed into RNase/DNase free CRYOGEN Tube 2.0 mL (Biosigma S.p.A.), weighed, immediately snap-frozen in liquid nitrogen, stored on dry ice and then in the freezer at ≤ -60 °C under monitored temperature conditions until transfer for further processing.

Animals euthanized due to reaching humane endpoint criteria were excluded from statistical analyses. Values from clinical biochemistry that were affected by hemolysis were also excluded from the analysis. The Benjamini-Hochberg multiple comparison correction was applied, and significance was accepted for data with an adjusted *p*-value bellow 0.05. A linear model was applied to each variable using the lm() function, implementing a two-way ANOVA to assess the effects of group, sex, and their interaction.

For the biodistribution study non-GLP quantification of the human transgene *CTNNB1* on a DNA and RNA level was performed via ddPCR (Biorad). Results from DNA analysis are reported as copies of the target gene (*hCTNNB1*) per 1 µg of DNA. During target gene specific ddPCR method development the following parameters were determined: nominal value of *mGAPDH* was 845.8 *mGAPDH* copies per 2.5 ng of DNA, LLOQ (Lower limit of quantification) 5,298.8 hCTNNB1 copies per 1 µg DNA and LOD (Limit of detection) 5298.8 hCTNNB1 copies per 1 µg DNA. Acceptance criteria were more than 10,000 accepted droplets/well and fewer than 2 detectable copies in negative template control samples (NTC). Values of DNA level of biodistribution analysis from raw data were calculated as: *hCTNNB1*/1µg DNA= (copies per 20 µL well (FAM)/ copies per 20 µL well (HEX)) *Nominal value of *mGAPDH* per 1µg of DNA, where FAM channel detected *hCTNNB1* and HEX detected *mGAPDH*. Results from RNA analysis are reported as copies of the target gene (*hCTNNB1*) per copies of the reference gene (*mGAPDH*). For RNA detection LLOQ was 0.002025 *hCTNNB1*/mGAPDH and LOD 0.00129 *hCTNNB1*/mGAPDH. Values of RNA biodistribution analysis from raw data were calculated as follows: *hCTNNB1*/mGAPDH= copies per 20 µL well (FAM)/ copies per 20 µL well (HEX), where FAM channel detected *hCTNNB*1 and HEX channel detected *mGAPDH*.

A GLP-like single dose biodistribution and toxicity study in non-human primates

For the single dose biodistribution and toxicity study, 2-4-year-old naïve cynomolgus macaques (*Macaca fascicularis*) were used. The study (90-day long) was conducted as a non-GLP study, following RD 53/2013 national approval. All non-human primates used in the study have been tested by the supplier for several distinct kind of infectious diseases, including tuberculosis, Herpes B virus infection, Simian Immunodeficiency Virus, salmonella, *Shigella* and filovirus. Nevertheless, animals were isolated for a minimum of 40 days. On day 1 of the study, the ICV administration of the test item (volume of the AAV suspension) was performed using ventriculography-assisted (X-Ray tube SR 90r20 FN (Siemens)) stereotactic surgery (86,87) using Stereotaxic frame 1730 (David Kopf Instruments), and Hamilton syringes. In brief, once the animals were located in the stereotaxic frame the skin above the skull was opened and a craniotomy was performed to visualize the mid-sagittal sinus. A pediatric spinal needle 25GA 3.50 IN 0.50 x 90 mm (Beckton Dickinson, cat# 405257,) coupled to a 1 ml syringe without dead volume (NIPRO, cat# SY3-1LC;) was orthogonally inserted 1.3 mm lateral to the midline until reaching the right lateral ventricle location confirmed by CSF aspiration followed by an x-ray plate with contrast agent (0.3 ml; Omnigraph®). Once location of the injection device was secured, the AAV suspension was delivered in pulses of 0.3 ml/min, and once completed, the needle was left in place for an additional time of 10 min before withdrawal, to avoid reflux of the AAV suspension through the injection tract. The same procedure was repeated for deliveries into the left lateral ventricle. For ICV administration (AP -0.2, ML -13.2, DV 3.517) (88), a midsagittal injection was performed to deliver 3.15×10^{13} or 7.85×10^{13} vg/dose of test item by bilateral ICV injection (2×2 mL, or 2×4 mL). Another group of animals was subjected to ICM injection (AP -0.2, ML -27.3, DV -18.7). In this case, the skin of the neck was opened, and muscles were separated by planes until securing a direct visualization of the cisternae magna in between the end of the occipital bone and the posterior lamina of the C1 vertebra. Next, the injection device (same as for ICV deliveries) was inserted in the midline of the cisternae magna with the help of a stereotaxic micromanipulator at a depth of 2 mm from the surface. The location of the injection device (same one as for ICV injections) inside the CSF space was confirmed by x-ray plates and by the extraction of a CSF volume equivalent to the AAV suspension to be delivered. Delivery was conducted in pulses of 0.3 m/min, and once completed, the injection needle was left in place for 10 minutes before

withdrawal to ensure the lack of reflux of the AAV suspension through the perforated dura matter. The hole made at the level of the dura matter was closed immediately upon needle removal by applying a pulse of the electrocoagulator. Once surgery was completed, each animal was returned to an individual cage until full recovery of the anesthesia. For ICM the animals received 3.15×10^{13} vg/dose of the test item, Urbagen, in 4 mL.

Body weight and neurological status were monitored throughout the study. On day 90, animals were euthanized and necropsies were performed following intracardiac perfusion with a phosphate buffer solution, with subsequent organ harvesting for histopathological H&E assessment. Perfusion was performed using fixative solution made of 3,000 mL of 4% paraformaldehyde and 0.1% glutaraldehyde in 0.1 M PB at neutral pH under a constant flow of 3,500 mL/h by the use of a Perfusion peristaltic pump 501S-170 (Watson-Marlow). Samples (frontal lobe, head of the caudate nucleus, basal ganglia, temporal lobe, thalamus, mesencephalon, hippocampus, pons, colliculi, occipital cortex, cerebellum, occipital cortex, visual cortex, spinal cord (cervical, thoracic & lumbar), and dorsal root ganglia (cervical, thoracic & lumbar), heart, liver (right lobe), lung (right lower lobe), kidney (right), spleen, gonads (testis or ovary), striatal skeletal muscle (quadriceps, right), skin (back), sciatic nerve (right), and median nerve (right)) were taken according to Pardo *et al*. (89) and embedded in the paraffin. Scoring for changes was carried out (Supplementary Table 13). Histopathological analyses in paraffin-embedded tissues were carried out by a reference pathologist with the credentials to perform GLP studies (Patconsult Lab). Blood (Vacutainer) was also collected for further analysis. A volume of 0.3 mL of cerebrospinal fluid (CSF) was collected by direct puncture of the cisternae magna with an insulin needle. CSF samples were quickly frozen in dry ice and stored at -80 ºC for further analysis.

From collected tissue non-GLP biodistribution analysis was performed via ddPCR (Biorad). During target gene specific ddPCR method development the following parameters were determined: nominal value of *mfGAPDH* was 692.3 *mfGAPDH* copies per 2.5 ng of DNA, LLOQ 3,084.4 hCTNNB1 copies per 1 µg DNA and LOD 3,084.4 hCTNNB1 copies per 1 µg DNA. Acceptance criteria were more than 10,000 accepted droplets/well with fewer than 2 detectable copies in NTC. Values of DNA level of biodistribution analysis from raw data were calculated as: *hCTNNB1*/1µg of DNA= (copies per 20 µL well (FAM)/ copies per 20 µL well (HEX)) *Nominal value of *mfGAPDH* per 1 µg of DNA, where FAM channel detected *hCTNNB1* and HEX channel detected *mfGAPDH*. Results from RNA analysis are reported as

copies of the target gene (*hCTNNB1*) per copies of the reference gene (*mfGAPDH*). For RNA detection LLOQ was 0.00023 hCTNNB1 / mfGAPDH and LOD 0.00023 hCTNNB1 / mfGAPDH. Values of RNA level of biodistribution analysis from raw data were calculated: *hCTNNB1*/mfGAPDH= copies per 20 µL well (FAM)/ copies per 20 µL well (HEX), where FAM channel detected hCTNNB1 and HEX channel detected *mfGAPDH*.

Study approval

Patient primary cells were obtained through the CTNNB1 Foundation, Slovenia and control cells were obtained through the Stem Cell and Organoid Facility at Children's Medical Research Institute, Australia. Written informed consent was filled prior to participation in this study, and samples were received and maintained in an anonymous manner. The protocol was approved by the Sydney Children's Hospital Network Human Research Ethics Committee under protocol 2024/ETH00133.

The efficacy study (C0010223) performed at Charles River Laboratories, Finland, was approved by the National Animal Experiment Board. The mouse study performed at the Westmead Medical Research Institute, Australia (8-month non-GLP study, Protocol No. 4385.03.23) was approved by the Western Sydney Local Health District Animal Ethics Committee, and the biodistribution and toxicology studies conducted at the Czech Centre for Phenogenomics, BIOCEV – Institute of Molecular Genetics, Prague (20-, 90-, 180-day studies, Protocol No. 5509/2024), were approved by the IACUC and the Resort Professional Commission of the CAS for Approval of Projects of Experiments on Animals. Studies carried out in NHPs (toxicology and biodistribution) were conducted in full keeping with the EU Council Directive 2010/63/UE and Spanish legislation in place (RD53/2013). Animal experimentation was approved by the Ethical Committee for Animal Testing of the University of Navarra (ref: 075-23) and by the Department of Animal Welfare of the Government of Navarra (ref: R-075-23GN).

Data availability

All underlying data and any supporting analytic code in this paper if available from the corresponding author upon request through email (llisowski@cmri.org.au, spela@ctnnb1-foundation.org).

Acknowledgments

This work was funded by the CTNNB1 Foundation, Slovenia, The Gene Therapy Research Institute, Slovenia and Children's Medical Research Institute (CMRI), Australia. Additionally, it was supported by the Ministry of Education, Science, and Innovation of the Republic of Slovenia through a research grant (no. 3360-24-03363), Slovenian Research Agency grant (J7-4537) as well as by generous donations from CTNNB1 families as well as general public, whose support made this research possible. We gratefully acknowledge the Stem Cell and Organoid Facility and the Imaging Facility at Children's Medical Research Institute (Australia) for their contributions to the *in vitro* studies, and the Westmead Institute for Medical Research (Australia) for providing the essential resources, infrastructure, and services required to conduct *in vivo* studies and analyze *in vitro* and *in vivo* experiments. The authors also acknowledge support from Luminesce Alliance. We sincerely thank Timotej Sotošek (NIC), Carmen L. Garreta-Celemin (CMRI), Deborah Nazareth (CMRI), Deborah Chandra (CMRI), Ramon Roca-Pinilla (CMRI), Sophia Liao (CMRI), Cindy Zhu (CMRI), Renina Gale Navarro (CMRI) and Santiago Mesa-Mora (CMRI) for valuable technical assistance, as well as Petra Sušjan (NIC) and Ruud Bueters (3D Pharma) for their contributions and collaboration. We are also grateful to The Jackson Laboratory for providing the initial mouse breeders for the efficacy study, and to Charles River Laboratories (Finland) and the Centre for Applied Medical Research (CIMA, Spain) for conducting the animal studies. We also thank Viralgen for the production of the vectors used for the toxicology and biodistribution studies, and Labena for acquiring the data from these studies. The authors used services of the Czech Centre for Phenogenomics at the Institute of Molecular Genetics supported by the Czech Academy of Sciences RVO 68378050 and by the project LM2023036 Czech Centre for Phenogenomics provided by Ministry of Education, Youth and Sports of the Czech Republic. We thank Excellence Hub for Advancing Innovation in Gene Therapy-GeneH grant 101186939) for funding part of the toxicology analysis. Figures were created with BioRender.com.

Author contributions

LL, ŠM, API and DL designed the research studies. API designed and conducted *in vitro* and *in vivo* studies, and acquired and analyzed the data with the help of HP. ŠM, AGH, RCS and DL contributed to the design of the efficacy study, and DL with the help of RJ analyzed the data from the mouse efficacy study. ŠM and DL contributed to the design of the safety and biodistribution studies, and DL and API analyzed the data. EMZ performed ddPCR analysis. LL, ŠM, DO, API and DL wrote the manuscript with the help of other authors. CM, and JC contributed to the design of therapeutic construct candidates, conducted preliminary *in vitro* experiments, acquired data and analyzed the data. AK conducted some of the *in vivo* experiments. FDH performed RNA data analysis in patient-derived organoids. JLLP conducted the NHPs study. MK generated the *CTNNB1* KO HEK cell line used for the validation of the constructs. All authors discussed and commented the results. The order of authorship was determined by overall contributions and approved by all the authors.

Competing interests

The CTNNB1 Foundation holds an exclusive global license to the international patent application WO2025/094056 ("Gene Therapy for CTNNB1 Syndrome"), filed by Children's Medical Research Institute. ŠM is the founding president of the CTNNB1 Foundation and LL, API, CM and JC are listed as inventors on the patent application.

The other authors declare no competing interests.

References

1. Lopez-Rivera JA, Perez-Palma E, Symonds J, Lindy AS, McKnight DA, Leu C, et al. A catalogue of new incidence estimates of monogenic neurodevelopmental disorders caused by de novo variants. Brain. 2020;143(3):1099–105. doi:10.1093/brain/awaa051

2. Miroševič Š, Khandelwal S, Sušjan P, Žakelj N, Gosar D, Forstnerič V, et al. Correlation between Phenotype and Genotype in CTNNB1 Syndrome: A Systematic Review of the Literature. International Journal of Molecular Sciences. MDPI; 2022. doi:10.3390/ijms232012564

3. Žakelj N, Gosar D, Miroševič Š, Sanders SJ, Ljungdahl A, Kohani S, et al. Genotypic, functional, and phenotypic characterization in CTNNB1 neurodevelopmental syndrome. Hum Genet Genomics Adv. 2025 Oct;6(4):100483. doi:10.1016/j.xhgg.2025.100483

4. Huang L, Lu J, Wang Y, Sun L, Ding X. Familial Exudative Vitreoretinopathy and Systemic Abnormalities in Patients With *CTNNB1* Mutations. Investig Opthalmology Vis Sci. 2023 Feb 15;64(2):18. doi:10.1167/iovs.64.2.18

5. Sinibaldi L, Garone G, Mandarino A, Iarossi G, Chioma L, Dentici ML, et al. Congenital heart defects in *CTNNB1* syndrome: Raising clinical awareness. Clin Genet. 2023 Nov;104(5):528–41. doi:10.1111/cge.14404

6. Lee J, Yoo J, Lee S, Jang DH. CTNNB1-related neurodevelopmental disorder mimics cerebral palsy: case report. Front Pediatr. 2023 Jun 16;11:1201080. doi:10.3389/fped.2023.1201080

7. Srivastava S, Lewis SA, Cohen JS, Zhang B, Aravamuthan BR, Chopra M, et al. Molecular Diagnostic Yield of Exome Sequencing and Chromosomal Microarray in Cerebral Palsy: A Systematic Review and Meta-analysis. JAMA Neurol. 2022 Dec 1;79(12):1287. doi:10.1001/jamaneurol.2022.3549

8. Ligt J de, Willemsen MH, Bon BWM van, Kleefstra T, Yntema HG, Kroes T, et al. Diagnostic exome sequencing in persons with severe intellectual disability. N Engl J Med. 2012 Nov;367:1921–9.

9. Machon O, Backman M, Machonova O, Kozmik Z, Vacik T, Andersen L, et al. A dynamic gradient of Wnt signaling controls initiation of neurogenesis in the mammalian cortex and cellular specification in the hippocampus. Dev Biol. 2007 Nov;311(1):223–37. doi:10.1016/j.ydbio.2007.08.038 PubMed PMID: 17916349.

10. Maguschak KA, Ressler KJ. The dynamic role of beta-catenin in synaptic plasticity. Neuropharmacology. 2012 Jan;62(1):78–88. doi:10.1016/j.neuropharm.2011.08.032

11. Wu H, Barik A, Lu Y, Shen C, Bowman A, Li L, et al. Slit2 as a β-catenin/Ctnnb1-dependent retrograde signal for presynaptic differentiation. eLIFE. 2015;1–20. doi:10.7554/eLife.07266.001

12. Chenn A, Walsh CA. Regulation of Cerebral Cortical Size by Control of Cell Cycle Exit in Neural Precursors. Science. 2002 Jul 19;297(5580):365–9. doi:10.1126/science.1074192

13. Kwiatkowski AV, Weis WI, Nelson WJ. Catenins: playing both sides of the synapse. Current Opinion in Cell Biology. 2007. p. 551–6. doi:10.1016/j.ceb.2007.08.005 PubMed PMID: 17936606.

14. Bamji SX, Shimazu K, Kimes N, Huelsken J, Birchmeier W, Lu B, et al. Role of beta-Catenin in Synaptic Vesicle Localization and Presynaptic Assembly. Neuron. 2003;40:719–31.

15. Bamji SX, Rico B, Kimes N, Reichardt LF. BDNF mobilizes synaptic vesicles and enhances synapse formation by disrupting cadherin-β-catenin interactions. J Cell Biol. 2006 Jul;174(2):289–99. doi:10.1083/jcb.200601087 PubMed PMID: 16831887.

16. Tai CY, Mysore SP, Chiu C, Schuman EM. Activity-Regulated N-Cadherin Endocytosis. Neuron. 2007 Jun;54(5):771–85. doi:10.1016/j.neuron.2007.05.013

17. Liu J, Xiao Q, Xiao J, Niu C, Li Y, Zhang X, et al. Wnt/β-catenin signalling: function, biological mechanisms, and therapeutic opportunities. Signal Transduction and Targeted Therapy. Springer Nature; 2022. doi:10.1038/s41392-021-00762-6 PubMed PMID: 34980884.

18. Yang C, Iyer RR, Yu ACH, Yong RL, Park DM, Weil RJ, et al. β-catenin signaling initiates the activation of astrocytes and its dysregulation contributes to the pathogenesis of astrocytomas. Proc Natl Acad Sci U S A. 2012 Jul;109(18):6963–8. doi:10.1073/pnas.1118754109 PubMed PMID: 22505738.

19. Li XM, Dong XP, Luo SW, Zhang B, Lee DH, Ting AKL, et al. Retrograde regulation of motoneuron differentiation by muscle β-catenin. Nat Neurosci. 2008 Jul;11(3):262–8. doi:10.1038/nn2053 PubMed PMID: 18278041.

20. Fu AKY, Cheung ZH, Ip NY. β-catenin in reverse action [Internet]. 2008. p. 244–6. Available from: http://www.nature.com/natureneuroscience

21. Liebner S, Corada M, Bangsow T, Babbage J, Taddei A, Czupalla CJ, et al. Wnt/β-catenin signaling controls development of the blood–brain barrier. J Cell Biol. 2008 Nov 3;183(3):409–17. doi:10.1083/jcb.200806024

22. O'Roak BJ, Vives L, Girirajan S, Karakoc E, Krumm N, Coe BP, et al. Sporadic autism exomes reveal a highly interconnected protein network of de novo mutations. Nature. 2012 May;485(7397):246–50. doi:10.1038/nature10989

23. Satterstrom FK, Kosmicki JA, Wang J, Breen MS, De Rubeis S, An JY, et al. Large-Scale Exome Sequencing Study Implicates Both Developmental and Functional Changes in

the Neurobiology of Autism. Cell. 2020 Feb;180(3):568-584.e23. doi:10.1016/j.cell.2019.12.036

24. Zhuang H, Liang Z, Ma G, Qureshi A, Ran X, Feng C, et al. Autism spectrum disorder: pathogenesis, biomarker, and intervention therapy. MedComm. 2024 Mar;5(3):e497. doi:10.1002/mco2.497

25. Alexander JM, Vazquez-Ramirez L, Lin C, Antonoudiou P, Maguire J, Wagner F, et al. Inhibition of GSK3α,β rescues cognitive phenotypes in a preclinical mouse model of CTNNB1 syndrome. EMBO Mol Med. 2024 Sep;16(9):2109–31. doi:10.1038/s44321-024-00110-5 PubMed PMID: 39103699; PubMed Central PMCID: PMC11393422.

26. Maruna M, Sušjan-Leite P, Meško M, Miroševič Š, Jerala R. RNA trans-splicing to rescue β-catenin: A novel approach for treating CTNNB1-Haploinsufficiency disorder. Mol Ther Nucleic Acids. 2025 Sep;36(3):102680. doi:10.1016/j.omtn.2025.102680

27. Drouyer M, Merjane J, Nedelkoska T, Westhaus A, Scott S, Lee S, et al. Enhanced AAV transduction across preclinical CNS models: A comparative study in human brain organoids with cross-species evaluations. Mol Ther Nucleic Acids. 2024 Jul;35(3). doi:10.1016/j.omtn.2024.102264

28. Wu Z, Asokan A, Samulski RJ. Adeno-associated Virus Serotypes: Vector Toolkit for Human Gene Therapy. Mol Ther. 2006 Jul;14(3):316–27. doi:10.1016/j.ymthe.2006.05.009 PubMed PMID: 16824801.

29. Mendell JR, Al-Zaidy SA, Rodino-Klapac LR, Goodspeed K, Gray SJ, Kay CN, et al. Current Clinical Applications of In Vivo Gene Therapy with AAVs. Molecular Therapy. Cell Press; 2021. p. 464–88. doi:10.1016/j.ymthe.2020.12.007 PubMed PMID: 33309881.

30. Zhou X, Gao G, Owens RA, Lu Y, Calcedo R, Miller J, et al. Roles of Inverted Terminal Repeats (ITRs) and Capsid Proteins from Novel NHP AAVs in rAAV Mediated Gene Transfer. Mol Ther. 2005 Jul;11:S156. doi:10.1016/j.ymthe.2005.06.407

31. Blair HA. Onasemnogene Abeparvovec: A Review in Spinal Muscular Atrophy. CNS Drugs. 2022 Jul;36(9):995–1005. doi:10.1007/s40263-022-00941-1 PubMed PMID: 35960489.

32. Cong F, Schweizer L, Chamorro M, Varmus H. Requirement for a Nuclear Function of β-Catenin in Wnt Signaling. Mol Cell Biol. 2003 Jul;23(23):8462–70. doi:10.1128/mcb.23.23.8462-8470.2003 PubMed PMID: 14612392.

33. Hinderer C, Katz N, Buza EL, Dyer C, Goode T, Bell P, et al. Severe Toxicity in Nonhuman Primates and Piglets Following High-Dose Intravenous Administration of an Adeno-Associated Virus Vector Expressing Human SMN. Hum Gene Ther. 2018 Jul;29(3):285–98. doi:10.1089/hum.2018.015 PubMed PMID: 29378426.

34. Brown BD, Gentner B, Cantore A, Colleoni S, Amendola M, Zingale A, et al. Endogenous microRNA can be broadly exploited to regulate transgene expression according to tissue, lineage and differentiation state. Nat Biotechnol. 2007 Dec;25(12):1457–67. doi:10.1038/nbt1372

35. Azuma H, Paulk N, Ranade A, Dorrell C, Al-Dhalimy M, Ellis E, et al. Robust expansion of human hepatocytes in Fah−/−/Rag2−/−/Il2rg−/− mice. Nat Biotechnol. 2007 Aug;25(8):903–10. doi:10.1038/nbt1326

36. Dalkara D, Byrne LC, Klimczak RR, Visel M, Yin L, Merigan WH, et al. In Vivo–Directed Evolution of a New Adeno-Associated Virus for Therapeutic Outer Retinal Gene Delivery from the Vitreous. Sci Transl Med. 2013 Jun 12;5(189). doi:10.1126/scitranslmed.3005708

37. Kayumi S, Pérez-Jurado LA, Palomares M, Rangu S, Sheppard SE, Chung WK, et al. Genomic and phenotypic characterization of 404 individuals with neurodevelopmental disorders caused by CTNNB1 variants. Genet Med. 2022 Nov;24(11):2351–66. doi:10.1016/j.gim.2022.08.006 PubMed PMID: 36083290.

38. Liberzon A, Birger C, Thorvaldsdóttir H, Ghandi M, Mesirov JP, Tamayo P. The Molecular Signatures Database Hallmark Gene Set Collection. Cell Syst. 2015 Dec;1(6):417–25. doi:10.1016/j.cels.2015.12.004

39. Brault V, Moore R, Kutsch S, Ishibashi M, Rowitch DH, McMahon AP, et al. Inactivation of the β-catenin gene by *Wnt1-Cre* -mediated deletion results in dramatic brain malformation and failure of craniofacial development. Development. 2001 Apr 15;128(8):1253–64. doi:10.1242/dev.128.8.1253

40. Lainšček D, Forstnerič V, Miroševič Š. CTNNB1 syndrome mouse models. Mamm Genome. 2025 Jun;36(2):390–402. doi:10.1007/s00335-025-10105-3

41. Chew B, Ryu JR, Ng T, Ma D, Dasgupta A, Neo SH, et al. Lentiviral silencing of GSK-3β in adult dentate gyrus impairs contextual fear memory and synaptic plasticity. Front Behav Neurosci. 2015 Jun 23;9. doi:10.3389/fnbeh.2015.00158

42. Shan HM, Maurer MA, Schwab ME. Four-parameter analysis in modified Rotarod test for detecting minor motor deficits in mice. BMC Biol. 2023 Aug 17;21(1):177. doi:10.1186/s12915-023-01679-y

43. Vasireddy V, Maguire CA, Anderson DW, Ng C, Gong Y, Eichler F, et al. An in vitro and in vivo efficacy evaluation of gene therapy candidate SBT101 in mouse models of adrenomyeloneuropathy and in NHPs. Mol Ther - Methods Clin Dev. 2024 Dec;32(4):101354. doi:10.1016/j.omtm.2024.101354

44. Daci R, Flotte TR. Delivery of Adeno-Associated Virus Vectors to the Central Nervous System for Correction of Single Gene Disorders. Int J Mol Sci. 2024 Jan 15;25(2):1050. doi:10.3390/ijms25021050

45. Chen X, Dong T, Hu Y, De Pace R, Mattera R, Eberhardt K, et al. Intrathecal AAV9/AP4M1 gene therapy for hereditary spastic paraplegia 50 shows safety and efficacy in preclinical studies. J Clin Invest. 2023 May 15;133(10):e164575. doi:10.1172/JCI164575

46. Hinderer C, Bell P, Katz N, Vite CH, Louboutin JP, Bote E, et al. Evaluation of Intrathecal Routes of Administration for Adeno-Associated Viral Vectors in Large Animals. Hum Gene Ther. 2018 Jan;29(1):15–24. doi:10.1089/hum.2017.026

47. Tucci V, Kleefstra T, Hardy A, Heise I, Maggi S, Willemsen MH, et al. Dominant β-catenin mutations cause intellectual disability with recognizable syndromic features. J Clin Invest. 2014 Apr 1;124(4):1468–82. doi:10.1172/JCI70372

48. European Medicines Agency. ICH guideline M3(R2) on non-clinical safety studies for the conduct of human clinical trials and marketing authorisation for pharmaceuticals. In. 2009.

49. European Medicines Agency. Guideline on the quality, non-clinical and clinical aspects of gene therapy medicinal products. In. 2018.

50. European Medicines Agency. Guideline on quality, non-clinical and clinical requirements for investigational advanced therapy medicinal products in clinical trials. In. 2025.

51. European Medicines Agency. ICH S12 Guideline on nonclinical biodistribution considerations for gene therapy products - Step 5. In. 2023.

52. OECD. In: Test No. 408: Repeated Dose 90-Day Oral Toxicity Study in Rodents [Internet]. OECD Publishing; 2025 [cited 2026 May 24]. (OECD Guidelines for the Testing of Chemicals, Section 4). Available from: https://www.oecd.org/en/publications/test-no-408-

repeated-dose-90-day-oral-toxicity-study-in-rodents_9789264070707-en.html doi:10.1787/9789264070707-en

53. Duan D. Lethal immunotoxicity in high-dose systemic AAV therapy. Mol Ther. 2023 Nov;31(11):3123–6. doi:10.1016/j.ymthe.2023.10.015

54. Ma W, Wu Z, Zhao T, Xia Y, Qin J, Tian X, et al. Preclinical evaluation of AAV9-coSMN1 gene therapy for spinal muscular atrophy: efficacy and safety in mouse models and non-human primates. Mol Med. 2025 Apr 29;31(1):158. doi:10.1186/s10020-025-01207-4

55. Bey K, Deniaud J, Dubreil L, Joussemet B, Cristini J, Ciron C, et al. Intra-CSF AAV9 and AAVrh10 Administration in Nonhuman Primates: Promising Routes and Vectors for Which Neurological Diseases? Mol Ther - Methods Clin Dev. 2020 Jun;17:771–84. doi:10.1016/j.omtm.2020.04.001

56. Galvan A, Petkau TL, Hill AM, Korecki AJ, Lu G, Choi D, et al. Intracerebroventricular Administration of AAV9-PHP.B SYN1-EmGFP Induces Widespread Transgene Expression in the Mouse and Monkey Central Nervous System. Hum Gene Ther. 2021 Jun;32(11–12):599–615. doi:10.1089/hum.2020.301

57. Park HK, Cho JW, Lee BS, Park H, Han JS, Yang MJ, et al. Reference values of clinical pathology parameters in cynomolgus monkeys (*Macaca fascicularis*) used in preclinical studies. Lab Anim Res. 2016;32(2):79. doi:10.5625/lar.2016.32.2.79

58. Kowal EJK, Sakai Y, McGurk MP, Pasetsky ZJ, Burge CB. Sequence-dependent and -independent effects of intron-mediated enhancement learned from thousands of random introns. Nucleic Acids Res. 2025 Feb 8;53(4):gkaf097. doi:10.1093/nar/gkaf097

59. Le Hir H, Nott A, Moore MJ. How introns influence and enhance eukaryotic gene expression. Trends Biochem Sci. 2003 Apr;28(4):215–20. doi:10.1016/S0968-0004(03)00052-5

60. Wang HF, Feng L, Niu DK. Relationship between mRNA stability and intron presence. Biochem Biophys Res Commun. 2007 Mar;354(1):203–8. doi:10.1016/j.bbrc.2006.12.184

61. Le Hir H. The exon-exon junction complex provides a binding platform for factors involved in mRNA export and nonsense-mediated mRNA decay. EMBO J. 2001 Sep 3;20(17):4987–97. doi:10.1093/emboj/20.17.4987

62. Dong F, Jiang J, McSweeney C, Zou D, Liu L, Mao Y. Deletion of CTNNB1 in inhibitory circuitry contributes to autism-associated behavioral defects. Hum Mol Genet. 2016 Apr 30;ddw131. doi:10.1093/hmg/ddw131

63. Mendell JR, Al-Zaidy S, Shell R, Arnold WD, Rodino-Klapac LR, Prior TW, et al. Single-Dose Gene-Replacement Therapy for Spinal Muscular Atrophy. N Engl J Med. 2017 Nov 2;377(18):1713–22. doi:10.1056/NEJMoa1706198

64. Nidetz NF, McGee MC, Tse LV, Li C, Cong L, Li Y, et al. Adeno-associated viral vector-mediated immune responses: Understanding barriers to gene delivery. Pharmacol Ther. 2020 Mar;207:107453. doi:10.1016/j.pharmthera.2019.107453

65. Mingozzi F, High K. Immune Responses to AAV in Clinical Trials. Curr Gene Ther. 2007 Oct 1;7(5):316–24. doi:10.2174/156652307782151425

66. Harkins AL, Ambegaokar PP, Keeler AM. Immune responses to central nervous system directed adeno-associated virus gene therapy: Does direct CNS delivery make a difference? Neurotherapeutics. 2024 Jul;21(4):e00435. doi:10.1016/j.neurot.2024.e00435

67. Bharucha-Goebel DX, Todd JJ, Saade D, Norato G, Jain M, Lehky T, et al. Intrathecal Gene Therapy for Giant Axonal Neuropathy. N Engl J Med. 2024 Mar 21;390(12):1092–104. doi:10.1056/NEJMoa2307952

68. Dowling JJ, Pirovolakis T, Devakandan K, Stosic A, Pidsadny M, Nigro E, et al. AAV gene therapy for hereditary spastic paraplegia type 50: a phase 1 trial in a single patient. Nat Med. 2024 Jul;30(7):1882–7. doi:10.1038/s41591-024-03078-4

69. Pearson TS, Gupta N, San Sebastian W, Imamura-Ching J, Viehoever A, Grijalvo-Perez A, et al. Gene therapy for aromatic L-amino acid decarboxylase deficiency by MR-guided direct delivery of AAV2-AADC to midbrain dopaminergic neurons. Nat Commun. 2021 Jul 12;12(1):4251. doi:10.1038/s41467-021-24524-8

70. Davidoff AM, Ng CYC, Zhou J, Spence Y, Nathwani AC. Sex significantly influences transduction of murine liver by recombinant adeno-associated viral vectors through an androgen-dependent pathway. Blood. 2003;102(2):480–8. doi:10.1182/blood-2002-09-2889 PubMed PMID: 12637328.

71. Silva Lima B, Videira MA. Toxicology and Biodistribution: The Clinical Value of Animal Biodistribution Studies. Mol Ther - Methods Clin Dev. 2018 Mar;8:183–97. doi:10.1016/j.omtm.2018.01.003

72. Costa-Verdera H, Meneghini V, Fitzpatrick Z, Abou Alezz M, Fabyanic E, Huang X, et al. AAV vectors trigger DNA damage response-dependent pro-inflammatory signalling in human iPSC-derived CNS models and mouse brain. Nat Commun. 2025 Apr 18;16(1):3694. doi:10.1038/s41467-025-58778-3

73. Greenberg BM, Minassian B, Messahel S, Edgar VB, Lowden A, Dahshi H, et al. First-in-human high dose AAV9 intrathecal gene therapy for paediatric CLN7 disease: a phase 1, open-label, single ascending dose, non-randomised clinical trial. eBioMedicine. 2026 Jan;123:106044. doi:10.1016/j.ebiom.2025.106044

74. Tarrant JC, Savickas P, Omodho L, Spinazzi M, Radaelli E. Spontaneous Incidental Brain Lesions in C57BL/6J Mice. Vet Pathol. 2020 Jan;57(1):172–82. doi:10.1177/0300985819859878

75. Koo BS, Lee DH, Kang P, Jeong KJ, Lee S, Kim K, et al. Reference values of hematological and biochemical parameters in young-adult cynomolgus monkey (Macaca fascicularis) and rhesus monkey (Macaca mulatta) anesthetized with ketamine hydrochloride. Lab Anim Res. 2019 Dec;35(1):7. doi:10.1186/s42826-019-0006-0

76. Hordeaux J, Buza EL, Dyer C, Goode T, Mitchell TW, Richman L, et al. Adeno-Associated Virus-Induced Dorsal Root Ganglion Pathology. Hum Gene Ther. 2020 Aug 1;31(15–16):808–18. doi:10.1089/hum.2020.167

77. Hawley ZCE, Pardo ID, Cao S, Zavodszky MI, Casey F, Ferber K, et al. Dorsal root ganglion toxicity after AAV intra-CSF delivery of a RNAi expression construct into non-human primates and mice. Mol Ther. 2025 Jan;33(1):215–34. doi:10.1016/j.ymthe.2024.11.029

78. Huang Q, Chan KY, Wu J, Botticello-Romero NR, Zheng Q, Lou S, et al. An AAV capsid reprogrammed to bind human transferrin receptor mediates brain-wide gene delivery. Science. 2024 Jun 14;384(6701):1220–7. doi:10.1126/science.adm8386

79. Giannelli SG, Luoni M, Iannielli A, Middeldorp J, Philippens I, Bido S, et al. New AAV9 engineered variants with enhanced neurotropism and reduced liver off-targeting in mice and marmosets. iScience. 2024 May;27(5):109777. doi:10.1016/j.isci.2024.109777

80. Strobel B, Miller FD, Rist W, Lamla T. Comparative Analysis of Cesium Chloride- and Iodixanol-Based Purification of Recombinant Adeno-Associated Viral Vectors for Preclinical Applications. Hum Gene Ther Methods. 2015 Aug;26(4):147–57. doi:10.1089/hgtb.2015.051

81. Cabanes-Creus M, Liao SHY, Gale Navarro R, Knight M, Nazareth D, Lau NS, et al. Harnessing whole human liver ex situ normothermic perfusion for preclinical AAV vector evaluation. Nat Commun. 2024 Mar 14;15(1):1876. doi:10.1038/s41467-024-46194-y

82. Cabanes-Creus M, Navarro RG, Zhu E, Baltazar G, Liao SHY, Drouyer M, et al. Novel human liver-tropic AAV variants define transferable domains that markedly enhance the human tropism of AAV7 and AAV8. Mol Ther - Methods Clin Dev. 2022 Mar;24:88–101. doi:10.1016/j.omtm.2021.11.011

83. Concordet JP, Haeussler M. CRISPOR: intuitive guide selection for CRISPR/Cas9 genome editing experiments and screens. Nucleic Acids Res. 2018 Jul 2;46(W1):W242–5. doi:10.1093/nar/gky354

84. Pasca S, Yoon SJ, Pasca S. Generation of Cortical Spheroids From Human Pluripotent Stem Cells. Protoc Exch. 2018 Dec. doi:10.1038/protex.2018.123

85. Guo Y, Chen J, Ji W, Xu L, Xie Y, He S, et al. High-titer AAV disrupts cerebrovascular integrity and induces lymphocyte infiltration in adult mouse brain. Mol Ther Methods Clin Dev. 2023 Dec;31:101102. doi:10.1016/j.omtm.2023.08.021

86. Lanciego JL, Luquin MR, Guillén J, Giménez-Amaya JM. Multiple neuroanatomical tracing in primates. Brain Res Protoc. 1998 Jun;2(4):323–32. doi:10.1016/S1385-299X(98)00007-5

87. Martin RF, Bowden DM. A Stereotaxic Template Atlas of the Macaque Brain for Digital Imaging and Quantitative Neuroanatomy. NeuroImage. 1996 Oct;4(2):119–50. doi:10.1006/nimg.1996.0036

88. Lanciego JL, Vázquez A. The basal ganglia and thalamus of the long-tailed macaque in stereotaxic coordinates. A template atlas based on coronal, sagittal and horizontal brain sections. Brain Struct Funct. 2012 Apr;217(2):613–66. doi:10.1007/s00429-011-0370-5

89. Pardo ID, Garman RH, Weber K, Bobrowski WF, Hardisty JF, Morton D. Technical Guide for Nervous System Sampling of the Cynomolgus Monkey for General Toxicity Studies. Toxicol Pathol. 2012 Jun;40(4):624–36. doi:10.1177/0192623311436180

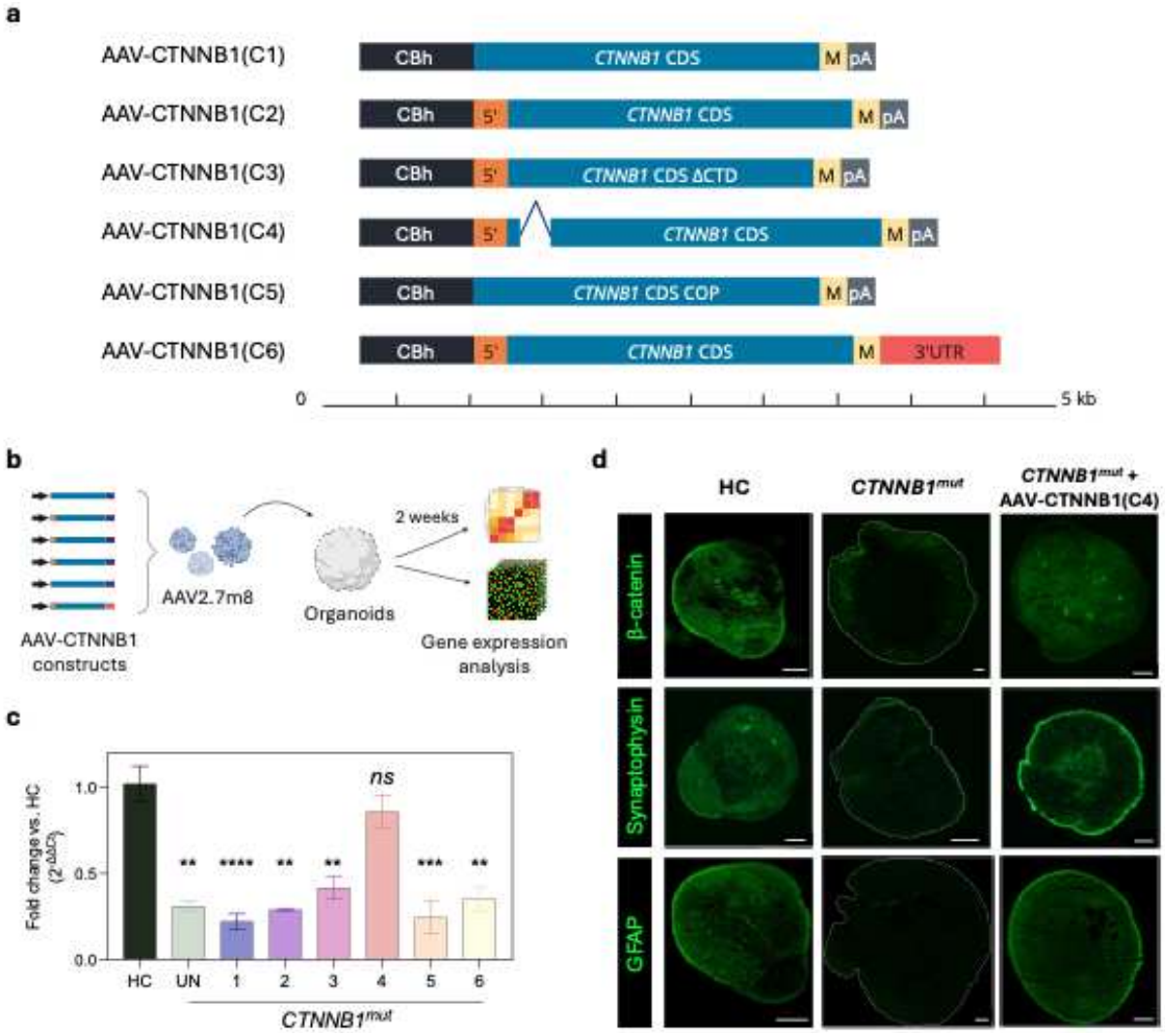


Figure 1. Rational selection of a potential therapeutic AAV cassette for CTNNB1 Syndrome. (**a**) Schematic representation of six AAV-CTNNB1 expression cassettes designed as candidates for *CTNNB1* gene augmentation. The expression of all the constructs is controlled by the cytomegalovirus/chicken β-actin hybrid (CBh) promoter and a polyadenylation site either derived from the bovine growth hormone gene or the endogenous *CTNNB1* gene (3'UTR). Complete natural, truncated (ΔCTD) and codon optimized (COP) versions of the *CTNNB1* coding DNA sequence (CDS) were assembled with different regulatory elements such as the endogenous 5'UTR (5'), intronic sequences, or microRNA-Targeting Sequences (M). The constructs were no longer than 4.9 kilobases (kb). (**b**) AAV-CTNNB1 construct screening workflow. Each construct was individually packaged into AAV2.7m8 capsids and vectors were used to transduce patient-derived cortical brain organoids. Two weeks after transduction, organoids were collected for gene expression analysis. (**c**) *CTNNB1* mRNA expression levels in patient-derived organoids either untreated (UN) or transduced with AAV-

CTNNB1 (C1-6) vectors at an MOT of 1.00×10^{10} vg/organoid. Data are shown as fold change (mean ± SEM) relative to the healthy control (HC), calculated using the $2^{-\Delta\Delta Ct}$ (Livak) method. Statistical comparisons were performed on $-\Delta\Delta Ct$, using one-way ANOVA (**** $p < 0.0001$) and Dunnett's multiple comparisons test (*ns*: non-significant, ** $p < 0.01$, *** $p < 0.001$, **** $p < 0.0001$). (**d**) Representative 20× immunofluorescence images of β-catenin, marker synaptophysin, and the Glial Fibrillary Acidic Protein (GFAP) in HC, and *CTNNB1*^{mut} organoids treated or not with AAV-CTNNB1(C4). Scale 200 µm.

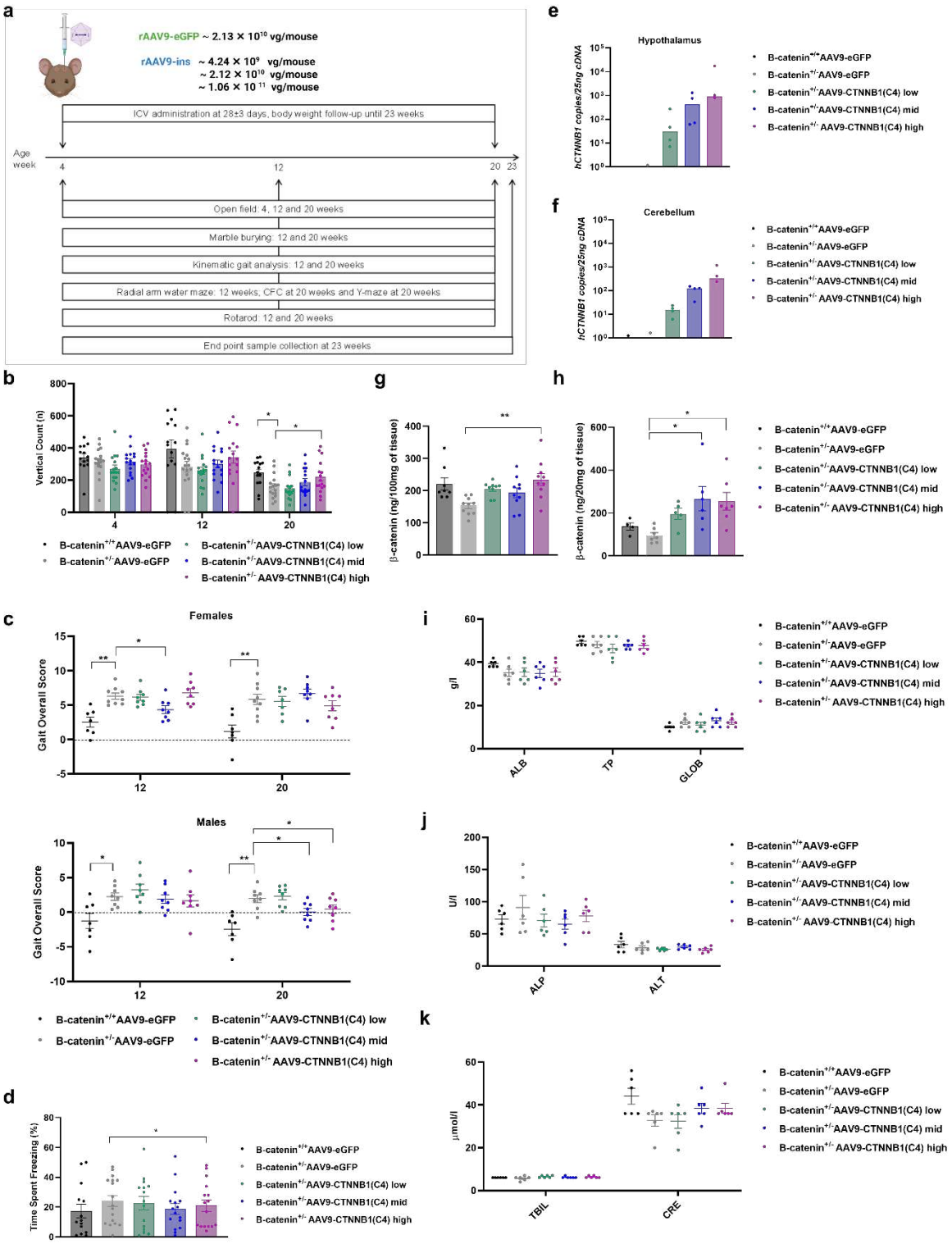


Figure 2: Determining the therapeutic efficacy of AAV9-CTNNB1(C4) in a CTNNB1 Syndrome mouse model. Beta-catenin$^{+/-}$ mice (n= 8-9/sex/group) were treated with low, mid, or high doses (4.29×10^9, 2.12×10^{10}, and 1.06×10^{11} vector genomes (vg)/mouse, respectively) of the test vector through the intracerebroventricular (ICV) route at 28±3 days-old and monitored for 20 weeks. An AAV9-eGFP control vector (2.12×10^{10} vg/mouse) was

administered to B-catenin$^{+/-}$ (n= 8-9/sex) and wild-type mice (n= 7/sex). (**a**) Efficacy study timeline. (**b**) Total rearing frequency in the open field for combined sexes at 4, 12 and 20 weeks of age (mean ± SEM; * $p < 0.05$ unpaired t-test). (**c**) Overall Kinematic Gait score determined at 12 and 20 weeks of age (mean ± SEM; * $p < 0.05$; ** $p < 0.01$; Two-way ANOVA with Tukey's multiple comparisons test). (**d**) Time Spent Freezing for combined sexes determined at 20 weeks of age by Contextual Fear Conditioning (mean ± SEM; * $p < 0.05$ unpaired *t*-test). (**e-f**) Human *CTNNB1* mRNA expression confirmed via RT-qPCR at the end of the study (n= 4/group; median). (**g-h**) Human β-catenin protein levels measured via ELISA in mouse brain left subcortex (**g**) and thalamus (**h**) (n= 4-7/group; mean ± SEM; * $p < 0.05$; ** $p < 0.01$; Two-way ANOVA with Tukey's multiple comparisons test). (**i-k**) Biochemical blood profile at the end of the study; albumin (ALB), total protein (TP) and globulins (GLOB) (**i**); liver enzymes Alanine Aminotransferase (ALT) and Alkaline Phosphatase (ALP) (**j**); and total bilirubin (TBI) and creatinine (CRE) (**k**) (n= 6-7/group).

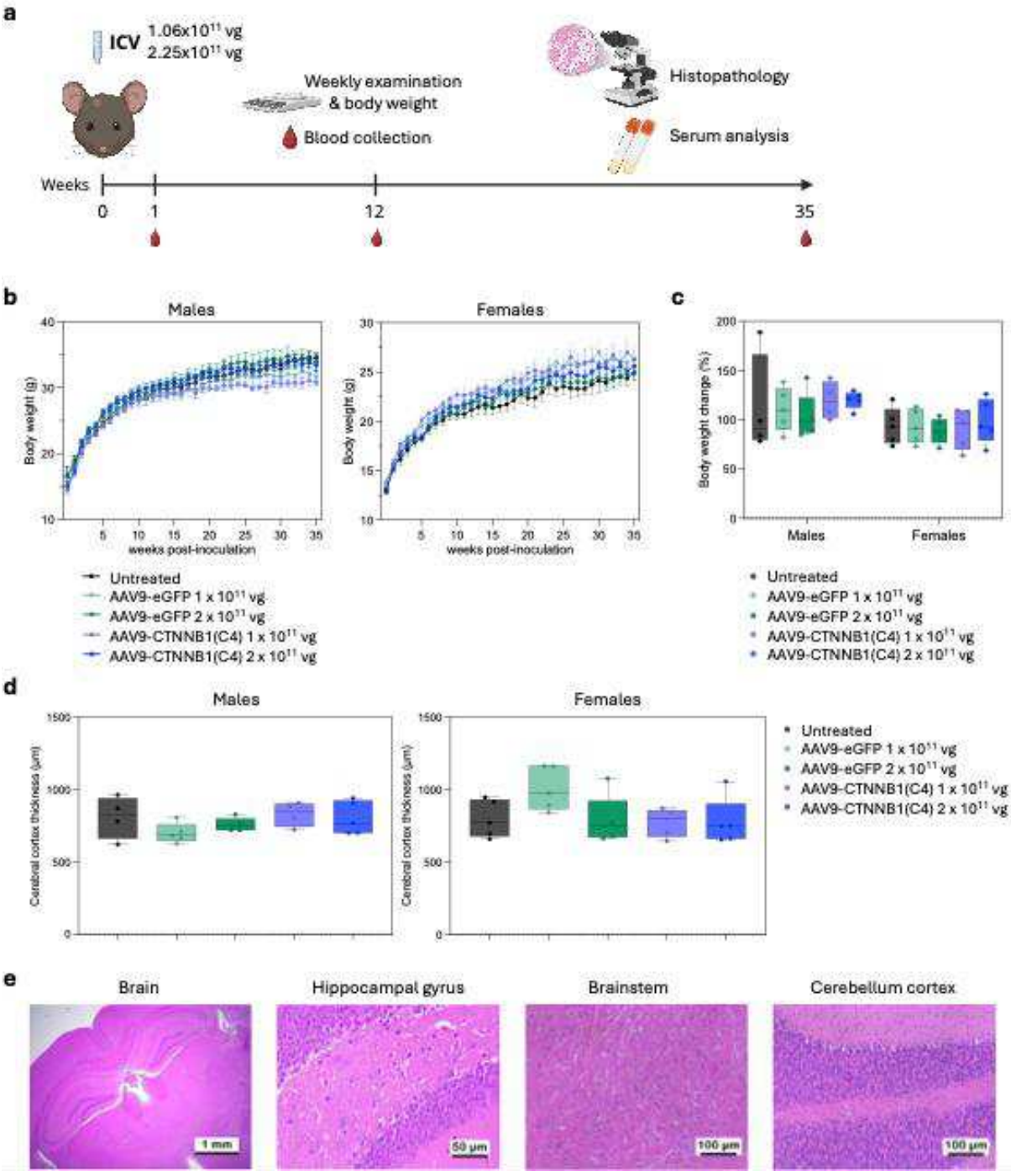


Figure 3. Long-term effects following intracerebroventricular (ICV) administration AAV9 in C57BL/6J mice. Wild-type mice (n = 5/vector/dose/sex) were administered either 1.06×10^{11} or 2.25×10^{11} vector genomes (vg) of the selected AAV9-CTNNB1(C4) or the AAV9-eGFP control vector and monitored for eight months. Untreated wild-type mice served as controls (n = 5/sex). (**a**) Overview of the 8-month study assessing vector tolerability. (**b**) Mouse body weights (mean ± SEM) were monitored weekly for up to 35 weeks post-treatment. Mixed-effects model (p= 0.2664) and two-way ANOVA (p= 0.2344) repeated measures were

used for statistical analysis in males and females, respectively. (**c**) Bodyweight changes (box=interquartile range, IQR; line within the box= median; whiskers= maximum and minimum). One-way ANOVA non-significant (p= 0.8732 for males and p= 0.9318 for females). (**d**) Cerebral cortex thickness (IQR; median; maximum and minimum values). One-way ANOVA (p= 0.2708) and Kruskal-Wallis (p= 0.1380) tests were used for statistical analysis in males and females, respectively. (**e**) Representative H&E histopathology images of the brain, hippocampal gyrus, brainstem, and cerebellum cortex. Scale bars 1 mm (brain), 50 µm (hippocampal gyrus), and 100 µm (brainstem and cerebellum).

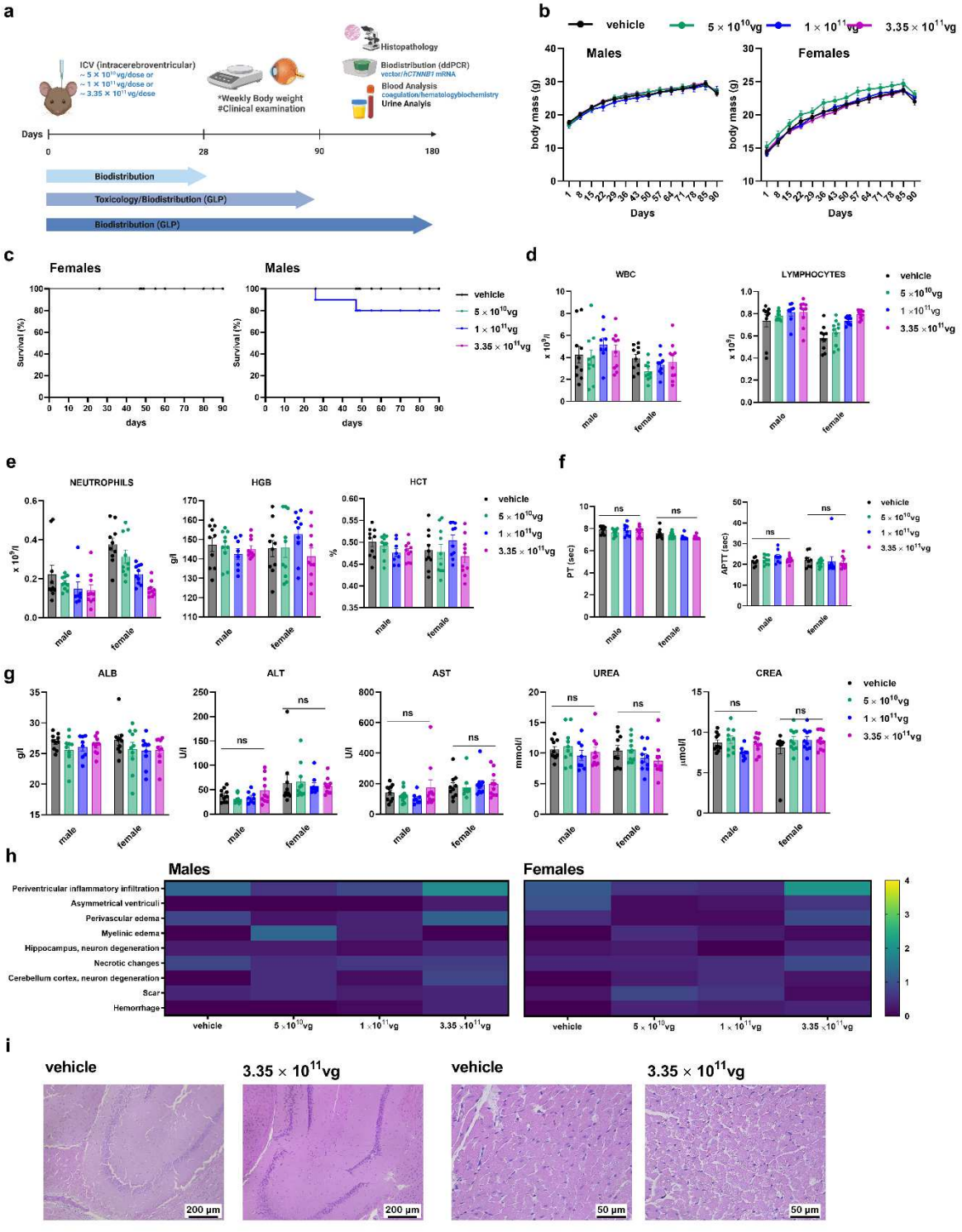
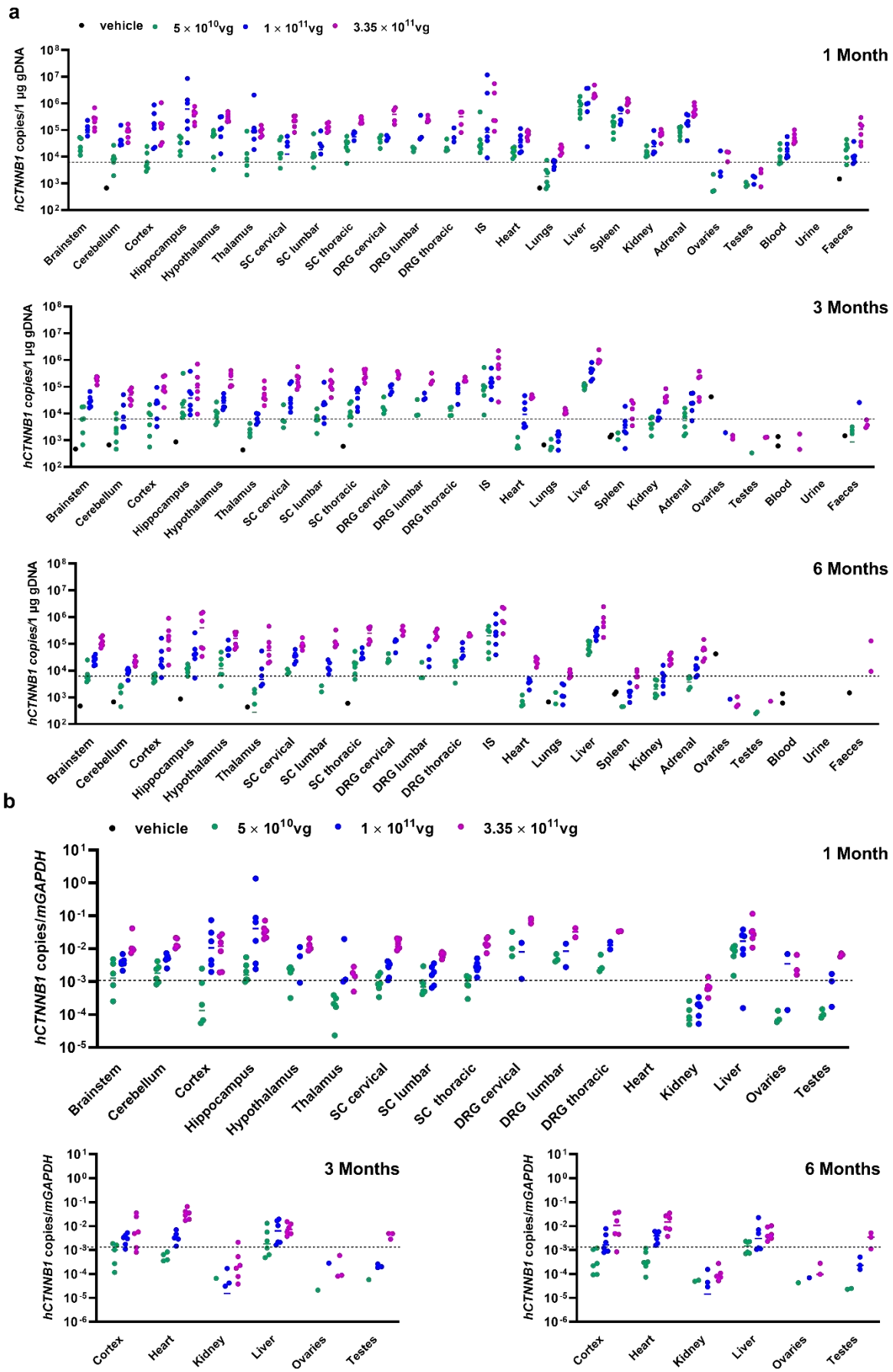


Figure 4: Overview of the 90-day GLP-toxicology study assessing the safety of Urbagen in wild-type mice. Wild-type C57BL/6NCrl mice were ICV inoculated with Urbagen at three different dose levels: low (5.00×10^{10} vg/mouse), mid (1.00×10^{11} vg/mouse), and high (3.35×10^{11} vg/mouse). Each group consisted of n= 10 mice/sex/dose and was evaluated over a 90-

day study period. (**a**) Experimental design of the *in vivo* toxicology and biodistribution studies. (**b**) Body weight progression of animals throughout the study. (**c**) Survival rates of animals in the toxicology study. (**d-e**) Differential blood count at day 90. WBC: White Blood Cells, HGB: Hemoglobin, HCT: Hematocrit. (**f**) Blood coagulation parameters at day 90. (**g**) Biochemical blood profile determined at the end of the study. ALB: Albumin, ALT: Alanine Aminotransferase, AST: Aspartate Aminotransferase, CREA: Creatinine kinase. (**h**) Histopathological scoring of brain alterations at study termination; mean values per group are shown for selected findings. (**i**) Representative H&E histopathology images of the brain and heart. Scale bars: ~200 µm (brain) and ~50 µm (heart). Data are presented as mean ± SEM; statistical significance was determined by two-way ANOVA followed by Tukey's multiple comparisons test).


a
vehicle
5 × 10^10 vg
1 × 10^11 vg
3.35 × 10^11 vg
1 Month
3 Months
6 Months
hCTNNB1 copies/1 µg gDNA
Brainstem
Cerebellum
Cortex
Hippocampus
Hypothalamus
Thalamus
SC cervical
SC lumbar
SC thoracic
DRG cervical
DRG lumbar
DRG thoracic
IS
Heart
Lungs
Liver
Spleen
Kidney
Adrenal
Ovaries
Testes
Blood
Urine
Faeces
b
vehicle
5 × 10^10 vg
1 × 10^11 vg
3.35 × 10^11 vg
1 Month
3 Months
6 Months
hCTNNB1 copies/mGAPDH
Brainstem
Cerebellum
Cortex
Hippocampus
Hypothalamus
Thalamus
SC cervical
SC lumbar
SC thoracic
DRG cervical
DRG lumbar
DRG thoracic
Heart
Kidney
Liver
Ovaries
Testes

1804

Figure 5: *In vivo* biodistribution of Urbagen in wild-type mice at different time points. Wild-type C57BL/6NCrl mice were ICV inoculated with Urbagen at low, mid, and high doses (5.00×10^{10}, 1.00×10^{11}, and 3.35×10^{11} vg/mouse, respectively; n=6/sex/dose). Using droplet digital PCR (ddPCR), biodistribution of the vector DNA (**a**) and transgene *hCTNNB1* mRNA expression (**b**) was determined at different time points (n= 3 animals/sex/dose).

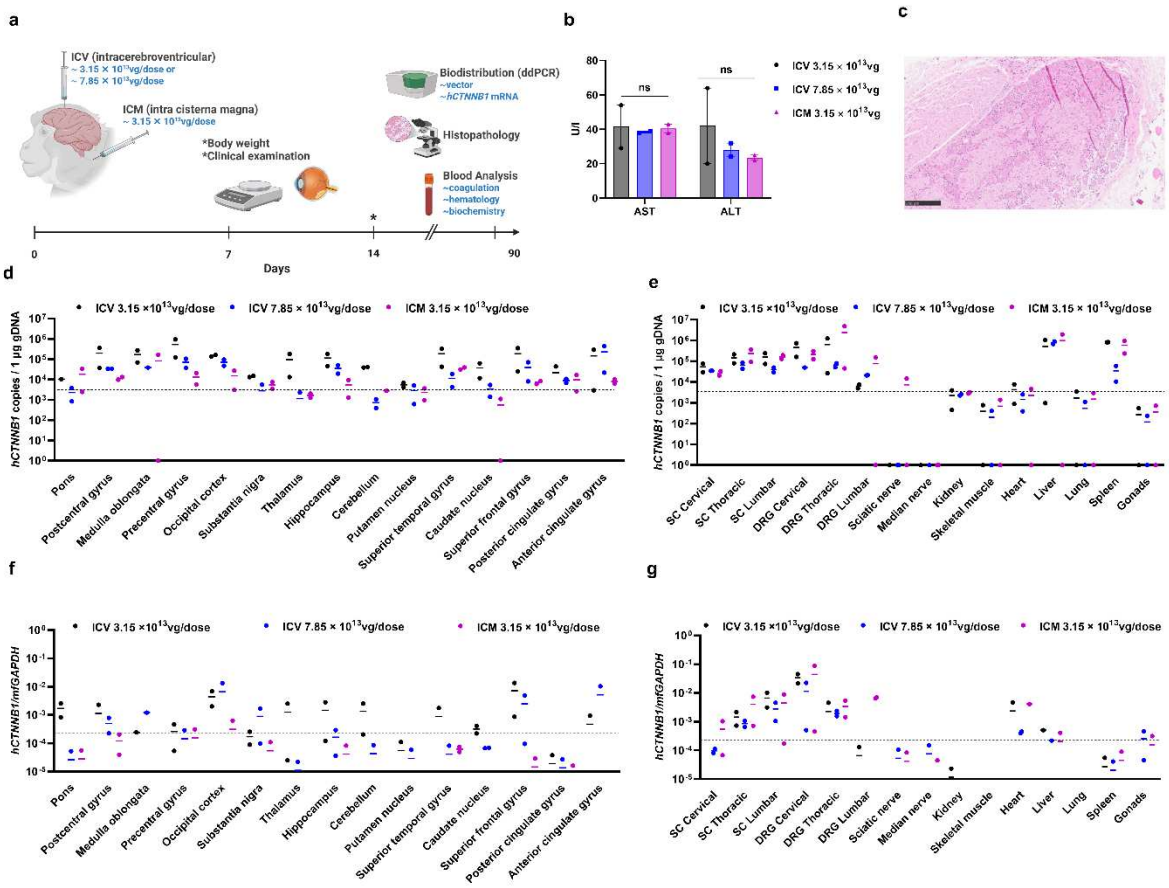


Figure 6: Ninety-day safety and biodistribution assessment in *Macaca fascicularis* following Urbagen administration. Nonhuman primates (NHPs; n=2/group) were treated with either 3.15×10^{13} or 7.85×10^{13} vg of Urbagen via stereotactic brain surgery using two different delivery approaches: biventricular ICV, or intracisterna magna (ICM). (**a**) Study timeline. (**b**) Liver enzymes (mean ± SEM, one-way ANOVA) measured at study end. (**c**) Representative cervical dorsal root ganglion section from an ICV-inoculated NHP (3.15×10^{13} vg). Scale bar: ~250 µm. (**d-e**) Vector biodistribution by ddPCR at study end in (**d**) brain regions and (**e**) peripheral tissues. *hCTNNB1* mRNA biodistribution by ddPCR at study end in (**d**) brain regions and (**e**) peripheral tissues. Vg: Vector genomes/NHP; AST: Aspartate aminotransferase; ALT: Alanine aminotransferase; SC: Spinal Cord; DRG: Dorsal Root Ganglion.

Supplementary Files

This is a list of supplementary files associated with this preprint. Click to download.

- PerezIturraldeSupplementaryInformation.pdf